Brain Structure and Function (2019) 224:387–417
https://doi.org/10.1007/s00429-018-1778-y

ORIGINAL ARTICLE

Aldosterone-sensitive HSD2 neurons in mice

Silvia Gasparini[1] · Jon M. Resch[2] · Sowmya V. Narayan[1] · Lila Peltekian[1] · Gabrielle N. Iverson[1] · Samyukta Karthik[1] · Joel C. Geerling[1]

Received: 25 May 2018 / Accepted: 3 October 2018 / Published online: 20 October 2018

Abstract

Sodium deficiency elevates aldosterone, which in addition to epithelial tissues acts on the brain to promote dysphoric symptoms and salt intake. Aldosterone boosts the activity of neurons that express 11-beta-hydroxysteroid dehydrogenase type 2 (HSD2), a hallmark of aldosterone-sensitive cells. To better characterize these neurons, we combine immunolabeling and in situ hybridization with fate mapping and Cre-conditional axon tracing in mice. Many cells throughout the brain have a developmental history of *Hsd11b2* expression, but in the adult brain one small brainstem region with a leaky blood–brain barrier contains HSD2 neurons. These neurons express *Hsd11b2, Nr3c2* (mineralocorticoid receptor), *Agtr1a* (angiotensin receptor), *Slc17a6* (vesicular glutamate transporter 2), *Phox2b*, and *Nxph4*; many also express *Cartpt* or Lmx1b. No HSD2 neurons express cholinergic, monoaminergic, or several other neuropeptidergic markers. Their axons project to the parabrachial complex (PB), where they intermingle with AgRP-immunoreactive axons to form dense terminal fields overlapping FoxP2 neurons in the central lateral subnucleus (PBcL) and pre-locus coeruleus (pLC). Their axons also extend to the forebrain, intermingling with AgRP- and CGRP-immunoreactive axons to form dense terminals surrounding GABAergic neurons in the ventrolateral bed nucleus of the stria terminalis (BSTvL). Sparse axons target the periaqueductal gray, ventral tegmental area, lateral hypothalamic area, paraventricular hypothalamic nucleus, and central nucleus of the amygdala. Dual retrograde tracing revealed that largely separate HSD2 neurons project to pLC/PB or BSTvL. This projection pattern raises the possibility that a subset of HSD2 neurons promotes the dysphoric, anorexic, and anhedonic symptoms of hyperaldosteronism via AgRP-inhibited relay neurons in PB.

Keywords Sodium appetite · Salt appetite · 11-Beta-hydroxysteroid dehydrogenase type 2 · Mineralocorticoid receptor · Aldosterone · Nucleus of the solitary tract · Angiotensin II · Dietary sodium · Dietary sodium deficiency · Dietary sodium deprivation

Introduction

Neurons in the nucleus of the solitary tract (NTS) receive life-critical information from the viscera about eating, drinking, breathing, and cardiovascular function. They integrate this information to control autonomic functions, mood, and behaviors (Parvizi and Damasio 2001; Craig 2002). The NTS is not a unitary brain nucleus. Instead, it contains diverse, intermingled subpopulations of neurons that modulate distinct functions like gastrointestinal motility, cardiac output, and breathing (Loewy and Spyer 1990; Chang et al. 2015).

Among these subpopulations is an unusual group that activates selectively in response to deficits in body sodium or extracellular fluid volume (Geerling et al. 2006a; Geerling and Loewy 2007c). These sodium depletion-activated neurons induce a behavioral state known as sodium appetite. Activating them causes mice to consume salt (Jarvie and Palmiter 2017; Resch et al. 2017). While their sources of synaptic input are unclear (Geerling and Loewy 2009; Resch et al. 2017), these neurons appear to sense two hormonal signals of sodium deficiency: aldosterone and angiotensin

Electronic supplementary material The online version of this article (https://doi.org/10.1007/s00429-018-1778-y) contains supplementary material, which is available to authorized users.

✉ Joel C. Geerling
joel-geerling@uiowa.edu

[1] Department of Neurology, University of Iowa, PBDB 1320, 169 Newton Rd., Iowa City, IA 52246, USA

[2] Department of Medicine, Beth Israel Deaconess Medical Center, Boston, USA

II (Geerling et al. 2006a; Geerling and Loewy 2006c, 2009; Resch et al. 2017).

Neurons in several other brain regions have angiotensin II receptors (Song et al. 1992), but what makes sodium depletion-activated NTS neurons special is that they also can detect aldosterone. Their aldosterone sensitivity led to their discovery and distinguishes them from most or all other neurons in the brain (Geerling et al. 2006b; Geerling and Loewy 2009). In addition to expressing the mineralocorticoid receptor (MR) like neurons in several other brain regions, these neurons express an enzyme required for cellular aldosterone-sensitivity, 11-beta-hydroxysteroid dehydrogenase type 2 (HSD2). HSD2 debulks the roughly 1000-fold higher concentration of glucocorticosteroids, which compete with aldosterone for MR binding in most cells (Funder et al. 1988; Naray-Fejes-Toth et al. 1998). HSD2, in addition to MR, is therefore a hallmark of all aldosterone-sensitive cells. In adult mice and rats, we refer to the subpopulation of NTS neurons expressing this enzyme as "NTS^{HSD2} neurons" (Resch et al. 2017) or simply "HSD2 neurons" (Geerling and Loewy 2006b; Jarvie and Palmiter 2017).

A decade after identifying and characterizing HSD2 neurons in rats, we and others switched to using Cre-conditional techniques in mice (Jarvie and Palmiter 2017; Resch et al. 2017). The opportunity for cell type-specific experiments outweighed several disadvantages of studying mice, including that sodium appetite in mice may be less mineralocorticoid dependent than in rats (Rowland and Fregly 1988). However, changing species necessitates a detailed examination of murine HSD2 neuroanatomy. Mice do have HSD2 neurons, but we lack detailed information about their other protein and mRNA expression, the full spectrum of brain regions to and through which their axons project, and whether any other brain regions contain aldosterone-sensitive cells. Over the past two decades, conflicting information has accumulated regarding which brain regions contain cells with *Hsd11b2* mRNA, HSD2 immunoreactivity, 11-beta-dehydrogenase activity, or aldosterone sensitivity (Jellinck et al. 1993; Sakai et al. 1996, 2000; Robson et al. 1998; Zhang et al. 2006; Geerling and Loewy 2007a, 2009; Naray-Fejes-Toth and Fejes-Toth 2007; Askew et al. 2015; Haque et al. 2015). Resolving these conflicts will allow us to focus effort on the specific brain circuit(s) that sense aldosterone to promote sodium appetite or to cause anhedonic and dysphoric symptoms during hyperaldosteronism in experimental animals (Grippo et al. 2006; Morris et al. 2006; Hlavacova and Jezova 2008; Hlavacova et al. 2012) and human patients (Malinow and Lion 1979; Sonino et al. 2006, 2011; Velema et al. 2017; Reincke 2018).

To resolve these conflicts, we combine sensitive techniques for detecting HSD2 protein and *Hsd11b2* mRNA in the adult brain, as well as Cre-lox fate mapping of past *Hsd11b2* expression. Next, to understand how cells inside the brain could detect a blood-borne peptide (angiotensin II) and a steroid that poorly penetrates the blood–brain barrier (aldosterone; Pardridge and Mietus 1979; Funder and Myles 1996; Geerling and Loewy 2009), we find that the HSD2 neuron distribution overlaps an NTS subregion with enhanced blood–brain barrier (BBB) permeability as shown by tissue infiltration of a blood-borne dye and endogenous proteins. We then confirm and expand our understanding of genetic markers identified using single-cell RNA-Seq (Resch et al. 2017) by immunolabeling proteins and using fluorescence in situ hybridization (FISH) to label mRNA transcripts relating HSD2 neurons to or distinguishing them from surrounding NTS neurons. Finally, after two studies showing the major HSD2 axon-terminal fields (Jarvie and Palmiter 2017; Resch et al. 2017), we confirm the basic findings of our conventional tracing experiments in rats (Geerling and Loewy 2006b) using Cre-conditional genetic tracing in two strains of *Hsd11b2* Cre-driver mice to label the full axonal arbors of HSD2 neurons and characterizing each major terminal field in detail. We also use dual retrograde tracing to test whether their axons branch or project separately to their two major target regions.

This expanded analysis confirms a lack of HSD2 outside the NTS in adult mice, identifies widespread cells with a developmental history of *Hsd11b2* expression, validates and reveals new genetic markers for HSD2 and other NTS neurons, and maps the detailed axonal projections of HSD2 neurons to targets in the brainstem and forebrain.

Materials and methods

Mice

All mice were group-housed in a temperature- and humidity-controlled room on a 12/12 h light/dark cycle and with ad libitum access to water and standard rodent chow (Envigo 7013). Unless otherwise specified, analyses were conducted in $n = 3$ male C57BL6/J (Jackson Laboratories) mice aged 8–16 weeks. In a subset of cases, we switched mice to a low-sodium chow (TD-130591, Teklad/Envigo) for a week to boost expression of *Hsd11b2*/HSD2. We also used a variety of knockin-Cre and Cre-reporter mice and a transgenic GFP reporter strain. Detailed information about each strain is provided in Table 1. All Cre-driver and -reporter mice were hemizygous and maintained on a C57BL6/J background. All experiments were conducted in accordance with the guidelines of the Institutional Animal Care and Use Committees at the University of Iowa or Beth Israel Deaconess Medical Center.

Table 1 Cre-driver and -reporter mice used in this study

Strain	References	Source information	Key gene
Hsd11b2^{Cre}	Jarvie and Palmiter (2017)	Jax 030545 http://www.informatics.jax.org/allele/key/871609	IRES-Cre-GFP inserted after the termination codon of *Hsd11b2*
Hsd11b2-Cre	Naray-Fejes-Toth and Fejes-Toth (2007) and Resch et al. (2017)	Available from originating investigators http://www.informatics.jax.org/allele/key/52180	Improved Cre (iCre) replaced a segment of exon1 in *Hsd11b2* locus
Pdyn-IRES-Cre	Krashes et al. (2014)	Jax 027958 http://www.informatics.jax.org/allele/MGI:5562873	Ribosomal entry sequence (IRES) fused to Cre recombinase and inserted downstream of the endogenous *Pdyn* (prodynorphin) gene
Agtr1a-GFP	Gong et al. (2003) and Gonzalez et al. (2012)	Tg(Agtr1a-EGFP)NZ44Gsat; RRID:MMRRC_033059-UCD; back-crossed to C57BL/J by T. Milner and then J. Grobe http://www.gensat.org/imagenavigator.jsp?imageID=77317	BAC transgene in which EGFP is inserted immediately upstream of the coding sequence of *Agtr1a*
R26-LSL-L10GFP reporter	Krashes et al. (2014)	Available from originating investigators http://www.informatics.jax.org/allele/MGI:5559562	Floxed transcription STOP cassette followed by EGFP/Rpl10 fusion reporter gene under control of the CAG promoter targeted to the Gt(ROSA)26Sor locus
Ai9 tdTomato reporter	Madisen et al. (2010)	Jax 007909 http://www.informatics.jax.org/allele/MGI:3809523	tdTomato (red fluorescent protein) WPRE inserted after loxSTOPlox under control of a CAG promoter between exons 1 and 2 of the Gt(ROSA)26Sor locus
Ai75 nuclear-tdTomato reporter	Allen Institute for Brain Science https://www.biorxiv.org/content/biorxiv/early/2017/11/25/224881.full.pdf	Jax 025106 http://www.informatics.jax.org/allele/MGI:5603432	tdTomato with amino-terminal addition of a 30 bp nuclear localization signal (NLS) under control of a CAG promoter and followed by WPRE was inserted after loxSTOPlox at the Rosa26 locus

Stereotaxic injections

Mice were anesthetized with isoflurane 0.5–1.5% (titrated to respiratory depth and rate ~ 40–80 breaths per minute with a deep surgical plane of anesthesia) or with an intraperitoneal (i.p.) injection combination of ketamine (100 mg/kg) plus xylazine (10 mg/kg) in 0.9% saline, then placed into a stereotaxic apparatus (Kopf 1900 or 940) with the head angled down. After a midline incision, we retracted skin and muscle to expose the atlanto-occipital membrane atop the cisterna magna, then used a 28-gauge needle or scalpel to incise it, providing access to the dorsal medulla. Through a pulled glass micropipette (20–30 µm inner diameter), we injected 90–200 nL of adeno-associated virus (AAV) into sites that were rostral 0.30 mm, lateral 0.15 mm, and ventral 0.3–0.5 mm relative to calamus scriptorius. Each injection was made slowly, over a 5-min period, using picoliter air puffs through a solenoid valve (Clippard EV 24VDC) pulsed by a Grass stimulator. The pipette was left in place for an additional 3 min then withdrawn slowly before closing the muscle with absorbable suture and skin with Vetbond (3M). Sustained release Meloxicam (1 or 4 mg/kg s.c.) was provided for postoperative analgesia. We injected $n = 4$ *Hsd11b2-Cre* mice with AAV8-Ef1a-DIO-synaptophysin-mCherry (Syp-mCherry; developed by Dr. Rachel Neve at the Massachusetts Institute of Technology McGovern Institute for Brain Research Viral Vector Core) and $n = 3$ *Hsd11b2-Cre* mice with AAV9-EF1a-DIO-ChR2(H134R)-mCherry (Chr2-mCherry; purchased from the University of Pennsylvania Vector core; donating investigator, Dr. Karl Deisseroth). We later injected $n = 4$ mice from a separate Cre-driver strain (*Hsd11b2*^{Cre}) with AAV8-Ef1a-DIO-Syp-mCherry. AAV-injected mice were allowed to survive for 3–4 weeks after surgery for optimal production and transport of Cre-conditional fluorescent proteins into axons.

For dual retrograde tracing, we made stereotaxic pressure injections of Fluorogold into the bed nucleus of the stria terminals and of cholera toxin b subunit (CTb) into the parabrachial complex. We used C57BL6/J male mice ($n = 2$) and *Hsd11b2-Cre; R26-lsl-Ai9-tdtomato* reporter mice ($n = 2$). The C57BL/6J mice received two, 45 nL injections of Fluorogold (2% w/v in PBS; Fluorochrome) into the right-side BST (rostral 0.1 mm, lateral 0.9 mm; 4.65 and 4.75 mm ventral to bregma) and two, 45 nL injections of cholera toxin B subunit (CTb 0.1% in distilled water; #103B, List Biological Laboratories) into the right-side parabrachial complex (caudal − 5.05 mm, lateral 0.9 mm; 3.75 and 3.85 mm ventral to bregma). The Ai9 (tdtomato) Cre-reporter mice received one 100 nL injection of Fluorogold into the BSTvL (rostral 0.2 mm, lateral 0.9 mm; ventral 4.8 mm) and one 100 nL injection of CTb into the parabrachial complex (caudal − 5.4 mm, lateral 1.3 mm; ventral 3.4).

Fluorogold i.p. injections

We combined Fluorogold 2% stock aliquots for volumes of 5, 10, 30, and 60 µL, then added PBS to a total injection volume of 300 µL (final w/v concentrations were 0.03, 0.07, 0.2, 0.4% Fluorogold). We injected these solutions intraperitoneally (i.p., left lower quadrant) in adult, male C57BL/6J mice ($n = 4$), which were perfused the next day for immunohistology as described below. The 5 µL (0.03%) injection case had no labeling in any tissue, cells, or blood vessels in the brain, so it was excluded from further analysis. The other $n = 3$ cases had qualitatively similar labeling in the dorsal vagal complex; the images presented here are from the 0.4% injection.

Brain tissue preparation

Under deep anesthesia with either ketamine–xylazine (i.p. 150–15 mg/kg) or 7% chloral hydrate (500 mg/kg, Sigma), all mice were perfused transcardially with PBS followed by 10% formalin-PBS (Fisher Scientific). After perfusion, we removed the brain and fixed it overnight in 10% formalin-PBS, then submerged it in 30% sucrose-PBS. Using a freezing microtome, we sectioned brains in the axial or sagittal plane at 40 µm. We collected separate, 1-in-3 tissue series in a cryoprotectant solution and stored them at − 20 °C until further processing. We sectioned some cases on a cryostat at 30 µm and collected 1-in-4 series.

Immunohistology

Detailed information on all primary antisera used in this study are in Table 2. For a few images, we used immunofluorescence protocols described previously (Resch et al. 2017), but most double-, triple-, and quadruple-labeled images shown here were labeled in a modified protocol, as follows. We removed tissue sections from cryoprotectant, rinsed them in PBS, and loaded them into a solution containing 1–4 primary antisera at the dilutions shown in the Table 2. These antisera were added serially to a PBS solution with 0.25% Triton X-100 (BP151-500, Fisher), 2% normal donkey serum (NDS, 017-000-121, Jackson ImmunoResearch), and 0.05% sodium azide (14314, Alfa Aesar) as a preservative (PBT-NDS-azide). All primary antisera were dilution tested (1:100–1:16,000 +) to minimize background labeling and optimize signal-to-noise for specific labeling of known objects of interest. Antisera targeting non-endogenous proteins (DsRed/mCherry, GFP, Fluorogold, CTb) do not produce cellular or axonal labeling in brain tissue from mice without injection of the respective neuroanatomical tracer, and in mice with tracer injections these antisera did not produce labeling in any brain region that was not already known to send or receive axons to or

Table 2 Antisera used in this study

Antigen	Immunogen description	Source, Host Species, RRID	Concentration
11-beta-hydroxysteroid dehydrogenase type 2 (HSD2)	Raised against amino acids 261–405 of the C-terminus of human 11β-HSD2	Santa Cruz, rabbit polyclonal, cat. #sc_20176, lot #B0609, AB_2233199	1:700
DsRed	DsRed-Express, a variant of *Discosoma* sp. red fluorescent protein	Clontech, rabbit polyclonal, cat. # 632496, lot #1509043, RRID: AB_1001313483	1:2000
mCherry	Full-length mCherry fluorescent protein	Life Sciences, rat monoclonal, cat. #M11217, lot #R1240561, RRID AB_2536611	1:2000
GFP	GFP isolated from *Aequorea victoria*	Invitrogen/Thermo Fisher, chicken polyclonal, cat. #PA1-9533, lot #1829565, RRID: AB_1074893	1:3000
Fluorogold	Fluorogold (glutaraldehyde conjugate)	Protos Biotech Corp, guinea pig polyclonal, cat. #NM-101, RRID: AB_2314409	1:500
Fluorogold	KLH-conjugated Fluorescent Gold	Millipore, rabbit polyclonal, cat. #AB153-I, lot #2905401, RRID: AB_2632408	1:2000
Cholera toxin B (CTB)	Purified choleragenoid, the B subunit of cholera toxin	List Biological, goat polyclonal, cat. #703, lot #7032A9, RRID: AB_10013220	1:10,000
Tyrosine hydroxylase (TH)	Purified, SDS-denatured rat pheochromocytoma tyrosine hydroxylase	Millipore, mouse monoclonal, cat.# MAB318, lot: NG1802536, RRID: 2201528	1:2000
Choline acetyltransferase (ChAT)	Human placental choline acetyltransferase	Millipore, goat polyclonal, cat. #AB144P, lot: JC1618187, RRID: AB_2079751	1:1000
Forkhead box protein 2 (FoxP2)	Recombinant human FOXP2 isoform 1 Ala640-Glu715	R&D Systems, sheep polyclonal, cat. #AF5647, RRID: AB_2107133	1:10,000
Paired-like homeobox 2b (Phox2b)	C-terminal region of mouse Phox2b	Hideki Enomoto, Kobe University, Japan, guinea pig polyclonal	1:12,000
LIM homeobox transcription factor 1 Beta (Lmx1b)	Full-length LIM homeobox transcription factor 1 beta protein from mouse	C. Birchmeier, Max Delbruck Center for Molecular Medicine; Berlin; Germany. RRID: AB_2314752	1:8000
Agouti-related protein (AgRP)	Human AGRP 83–132 amide	Phoenix, rabbit polyclonal, cat. # H-00353, lot: 01756, RRID AB_2313908	1:5000
Calcitonin gene-related polypeptide (CGRP)	Synthetic peptide corresponding to Rat CGRP (C-terminal sequence: VKDNFVPTNVGSEAF)	Abcam, goat polyclonal, cat: ab30061, lot: GR186007, RRID: AB_725807	1:10,000

from the injected region. The detailed pattern of labeling with the HSD2 antibody is described below and compared directly with Hsd11b2 mRNA expression (Results), replicating and extending prior findings in mice (Jarvie and Palmiter 2017; Resch et al. 2017). For some antisera, we verify direct correspondence between protein immunofluorescence and mRNA marker expression in several well-characterized cell types in the medulla, including catecholamine neurons (TH, *Slc18a2*), cholinergic neurons (ChAT, *Slc18a3*), and Phox2b/*Phox2b*. Labeling with FoxP2, Lmx1b, AgRP, CGRP, and other antisera conformed to patterns of neurons and axons already shown to produce these proteins in rats and mice, and we verified the labeling pattern for each with patterns of mRNA and protein labeling in the peer-reviewed neuroanatomical literature cited throughout the Results and Discussion of this paper and in the Allen Brain Atlas (http://www.brain-map.org). We did not use any antisera in this study that label neurons or axons in brain regions or patterns not previously established in the peer-reviewed neuroanatomical literature or Allen Brain Atlas.

We incubated sections overnight in this primary antibody solution at room temperature, on a tissue shaker. The next morning, after washing sections 3X in PBS, we incubated them for 2 h at room temperature in PBT-NDS-azide with 2–4 species-specific, affinity-purified, donkey secondary antisera conjugated to Cy3, Alexa Fluor 488, Cy5, or biotin (Jackson ImmunoResearch #s 711-065-152, 711-165-152, 711-175-152, 705-065-147, 705-545-147, 713-545-147,

706-545-148, 706-165-148, 706-065-148, 715-065-15, 712-165-153; each diluted 1:1,000 or 1:500). To label mouse IgG, we used Alexa-488-conjugated donkey anti-mouse IgG (H + L) without a preceding mouse primary antibody (Jackson #715-545-150; 1:500). Sections were then washed 3X in PBS and either mounted on glass slides or, in cases with a biotinylated secondary, incubated in streptavidin-Cy5 (1:500, #SA1011, Invitrogen) or streptavidin-Pacific Blue (1:750, #S11222, Life Technologies) in PBT-NDS-azide. After washing 3X in PBS, sections were mounted on glass slides (#2575-plus; Brain Research Laboratories) then coverslipped using Vectashield with DAPI (Vector Labs) or, if Pacific Blue was used, Vectashield without DAPI or Cytoseal 60 (#8310-4, Thermo Scientific). Most slides were imaged on the same day, then stored in slide folders at 4 °C.

For brightfield labeling (immunohistochemistry), we removed tissue sections from cryoprotectant, rinsed them in PBS, then incubated them in 0.3% hydrogen peroxide (#H325-100, Fisher) in PBT for 30 min to quench endogenous peroxidase activity. After 3X PBS washes, we loaded sections into PBT-NDS-azide with rabbit anti-HSD2 or anti-dsRed (dilutions in Table 2) overnight, at room temperature, on a tissue shaker. The next morning, after 3X PBS washes, we incubated sections for 2 h in a 1:500 solution of biotinylated donkey anti-rabbit (#711-065-152; Jackson) in PBT-NDS-azide. After three more PBS washes, sections were placed for 1 h in avidin–biotin complex (Vectastain ABC kit PK-6100; Vector), washed 3X in PBS, then incubated in diaminobenzidine (DAB) solution for 10 min. Our stock DAB solution was prepared by adding 100 tablets (#D-4418, Sigma, Saint Louis, MO) into 200 mL ddH2O, then filtering. We used 1 mL of this filtered DAB stock solution, with or without 300 µL of 8% nickel chloride (#N54-500, Fisher Chemical) per 6.5 mL PBS for coloration. After 10 min in DAB (or NiDAB), we added hydrogen peroxide (30%, 0.8 µL per 1 mL PBS-DAB) and swirled sections for 1–3 min until observing dark brown (DAB) or black (nickel-DAB) color change. After two rapid PBS washes, we wet-mounted one or more sections, checked them for optimal staining in a light microscope, and in rare cases, replaced sections for up to one additional minute of additional enzymatic staining. Finally, after washing sections 3X in PBS, we mounted them on glass slides. Slides were air-dried, then dehydrated in an ascending series of alcohols and xylenes, and coverslipped using Cytoseal.

Nissl counterstaining

After brightfield, whole-slide imaging, we removed coverslips from NiDAB-stained sections by immersing them overnight in xylenes. After rehydration (1-min dips in a graded series of alcohols), we rinsed slides in ddH2O then dipped them in a fresh, filtered solution of 0.125% thionin (Fisher Scientific) for up to 60 s. Slides were then rinsed in ddH2O with tap water until the solution cleared and then dehydrated serially in 50%, then 70% EtOH, fresh 95% EtOH (400 mL with ten drops of glacial acetic acid to clear excess thionin), 95%, 100%, and 100% EtOH, then two incubations in xylenes, from which we coverslipped each slide with Cytoseal.

Fluorescence in situ hybridization

To label mRNA for *Hsd11b2*, Vglut2/*Slc17a6, Phox2b, Nr2c3, Agtr1a, Cartpt, Nxph4a, Gal, Cck*, VMAT2/*Slc18a2*, VAChT/*Slc18a3* or Vgat/*Slc32a1*, we used RNAscope Fluorescent Multiplex Detection Reagents (ref# 320851, lot# 2002259; Advanced Cell Diagnostics) with probes listed in Table 3. For background cytoarchitecture, we labeled *Ubc* in some cases. Each observation reported here was confirmed in a 1-in-3 series of 40 µm tissue sections through the caudal NTS of $n = 3$ male C57BL/6J mice, unless otherwise noted.

The afternoon before hybridization, we removed sections from cryoprotectant and rinsed them in PBS at room temperature before mounting them on glass slides kept at 4 °C. In the morning, we used a Super-HI PAP pen (Research Products Incorporated) and vacuum grease (Dow Corning) to form a hydrophobic barrier around the sections and washed sections for 2 min in PBS twice at room temperature. We then covered sections with Protease IV and placed them on large glass petri dishes floating in a 40 °C water bath for 30 min. After two PBS 2 min washes, we incubated sections in one or more probes (Table 3) for 2 h at 40 °C. After that, we added amplification reagents Amp1-4 in series for 15–30 min each at 40 °C, with 2 × 2 min washes in RNAscope wash buffer (ref 320058, lot# 2001175) diluted 1:50 in ddH2O, between each step.

After Amp4, we either rinsed sections overnight with PBS at 4 °C to reduce wrinkles in the sections or performed an immunofluorescence protocol to label HSD2. For this, we incubated sections in a PBT-NDS-azide solution with rabbit anti-HSD2 (1:700) overnight at 4 °C. After washing with PBS the next morning, we added Cy3-conjugated donkey anti-rabbit (1:500; Jackson) for 2 h at room temperature. After a final PBS wash, we coverslipped slides using Vectashield with DAPI.

Imaging, counts, and figures

All slides were imaged with a 10 × or 20 × objective on an Olympus VS120 slide-scanning microscope. For brightfield images of DAB/NiDAB and Nissl-counterstained sections, we used extended focal imaging (EFI) to collect and combine in-focus light from all focal planes through the tissue. After reviewing whole-slide images in OlyVIA or VS-ASW software (Olympus), we collected additional EFI

Table 3 Fluorescence in situ hybridization probes used in this study

Probe	Common name	Channel	ACD Catalog #	Lot #
Mm-Agt	Angiotensinogen	C1	426941	18017A
Mm-Agtr1a-01	Angiotensin II receptor 1a	C1	481161	17172A
Mm-Apoe	Apolipoprotein E	C3	313271-C3	18017B
Mm-Cartpt	Cocaine and amphetamine-regulated transcript	C1	432001	17138B
Mm-Cck-C2	Cholecystokinin	C2	402271-C2	18017B
Mm-Gal-C3	Galanin	C3	400961-C3	17257B
Mm-Hsd11b2	11-beta-hydroxysteroid dehydrogenase type 2	C1	494891	17019A
Mm-Hsd11b2-C2	11-beta-hydroxysteroid dehydrogenase type 2	C2	494891-C2	17019B
Mm-Nxph4	Neurexophilin 4	C1	489641	16344B
Mm-Phox2b-C2	Paired-like homeobox 2b	C2	407861-C2	17013A
Mm-Slc17a6	Vesicular glutamate receptor 2	C1	319171	17251A
Mm-Slc18a2-C3	Vesicular monoamine transporter 2	C3	425331-C3	17303A
Mm-Slc18a3-C3	Vesicular acetylcholine transporter	C3	448771-C3	17349A
Mm-Slc32a1-C3	Vesicular GABA transporter	C3	319191-C3	18038A
Mm-Ubc	Ubiquitin C	C1	310771	18010A
Mm-Ubc-C2	Ubiquitin C	C2	310771-C2	18095B
Mm-Ubc-C3	Ubiquitin C	C3	310771-C3	18085A

or multifocal image stacks with the 20 × or 40 × objective in some regions of interest. For dual retrograde tracing (CTb + Fg) experiments, we counted double- and triple-labeled cells by scrolling up and down through 40x focal planes (12 µm stacks; 0.84 µm Z-spacing between each image) to confirm co-localization.

For mRNA co-localization, we used 20 ×–40 × image stacks to count HSD2-immunoreactive or *Hsd11b2* mRNA-expressing cells (denominator), only those containing a nucleus (DAPI) in the plane of section, and to score each neuron for the presence or absence of the co-labeled mRNA of interest. We set a conservative counting criterion of at least ten distinct fluorescent dots per cell (presumptive mRNA transcripts) for scoring individual *Hsd11b2*/HSD2 neurons, meaning that an individual neuron was scored as positive of gene expression of interest if and only if it contained at least ten distinct transcripts for the mRNA in question, within the same cytoplasm containing *Hsd11b2* mRNA or HSD2-ir surrounding that neuron's DAPI + nucleus and, in cases with ubiquitin mRNA labeling, also within the bounds of that neuron's dense cytoplasmic mRNA for *Ubc*. For all mRNA expression, the vast majority of HSD2 neurons contained either zero or many more than ten fluorescent dots (mRNA transcripts).

To prevent overcounting objects that span two tissue sections, we Abercrombie-corrected our HSD2 neuron counts using the average diameter of our criterion object, the nuclear diameter of HSD2 neurons (long-axis measurement), which ranged from 9.1 ± 0.1 µm ($n = 170$) in immunolabeled tissue or 9.4 ± 1.5 µm ($n = 42$) in mRNA-labeled tissue.

In every axon tracing case, we immunolabeled, imaged, Nissl-counterstained, reimaged, and examined all sections from least one 1-in-3 series through the full brain, from the olfactory bulbs to the cervical spinal cord. To construct the whole brain map of axonal projections, we manually traced axons and boutons with NiDAB immunolabeling for dsRed (Syp-mCherry) in Adobe Illustrator, then overlaid the Nissl-counterstained, re-scanned images of each section, which aided in labeling and outlining a minimal set of landmarks at each level for neuroanatomical clarity. We used neuroanatomical terminology from the peer-reviewed scientific literature (Geerling and Loewy 2006b; Shin et al. 2008; Geerling et al. 2010; Verstegen et al. 2017) and, for some well-established regions and neuron populations, from commercially available mouse brain atlases (Dong 2008; Franklin and Paxinos 2013). We used Adobe Photoshop to import raw fluorescence (grayscale) data into color channels for multicolor combinations, crop bitmap images, and adjust brightness or contrast. We added lettering and made drawings in Illustrator. Scalebars were traced atop calibrated lines in OlyVIA/VS-ASW to produce a simple white or black line.

Results

HSD2-immunoreactive neurons in the mouse brain

We immunolabeled HSD2, the enzyme required for cellular aldosterone sensitivity, in axial or sagittal sections through the full brains of C57BL/6J male mice ($n = 10$; 7–13 weeks, 22–29 g). We tested a range of primary antibody concentrations (1:100–1:4000) and used both immunofluorescence ($n = 6$) and, for maximal sensitivity, DAB and Ni-DAB immunohistochemistry ($n = 4$).

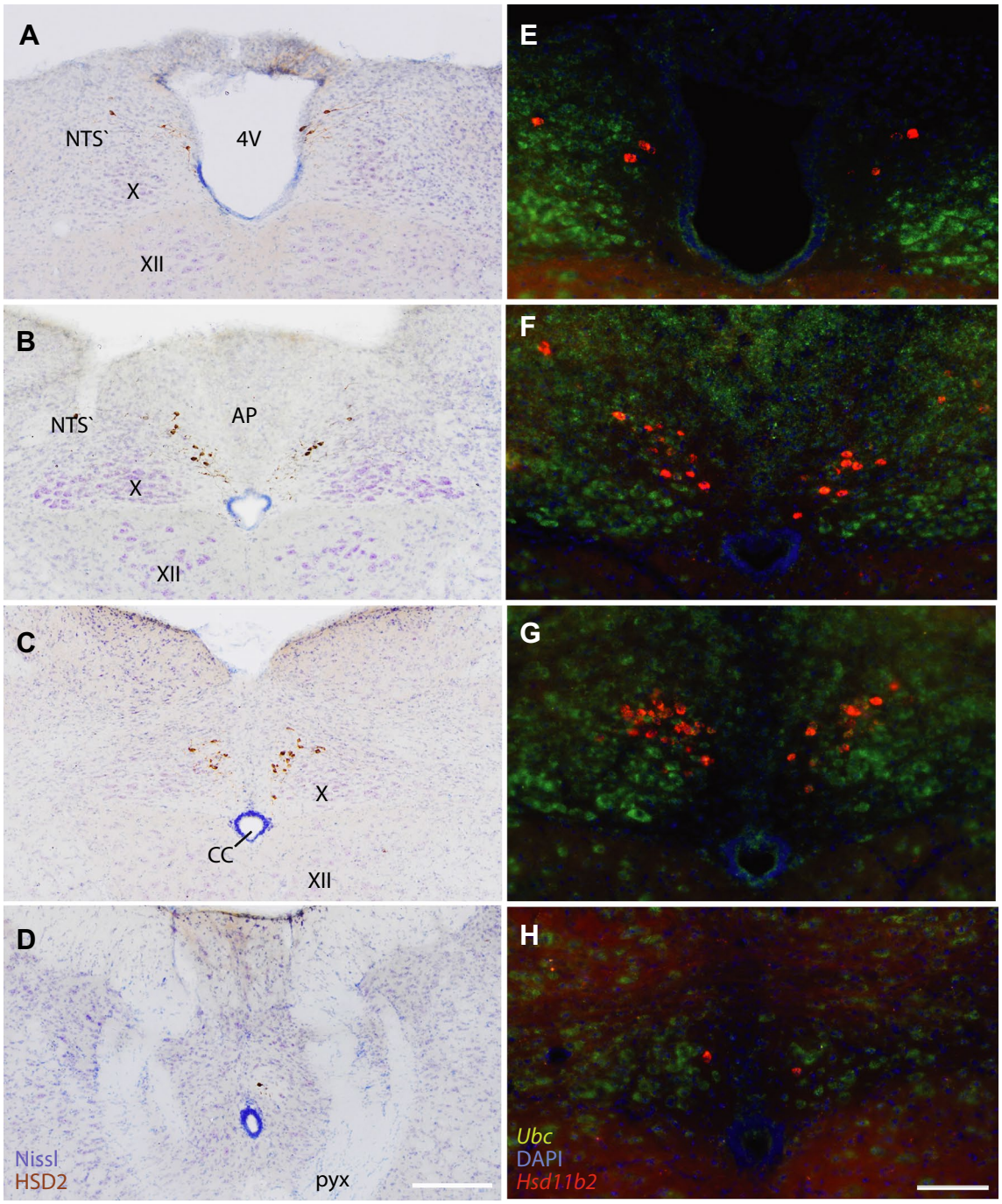

Fig. 1 **a–d** Diamidobenzidine (DAB) immunohistochemical staining for 11-beta-hydroxysteroid dehydrogenase type 2 (HSD2) at successively caudal levels of the dorsal medulla, with Nissl counterstain. **e–h** Fluorescence in situ hybridization for *Hsd11b2* (red–orange) at similar levels in a separate mouse. Ubiquitin C mRNA (*Ubc*, green) and nuclear labeling (DAPI, blue) are shown for cytoarchitectural reference. Scale bars are 200 µm (**a–d**) and 100 µm (**e–h**). *4V* fourth ventricle, *CC* central canal of the spinal cord, *NTS* nucleus of the solitary tract, *AP* area postrema, *X* dorsal motor nucleus of the vagus nerve, *XII* hypoglossal motor nucleus

The mouse NTS contains a small subpopulation of HSD2-immunoreactive neurons forming the same distribution in every brain (Fig. 1a–d). Their distribution parallels the distribution of *Hsd11b2* mRNA (Fig. 1e–h). The HSD2 neurons appear at the obex, along the wall of the fourth ventricle (Fig. 1a). HSD2 neurons at this level are sparse in mice, in contrast to the large rostral cluster in rats (Geerling et al. 2006b). The HSD2 neurons extend caudally in symmetric streaks beneath the area postrema (Fig. 1b), then gather into dense clusters immediately caudal to the

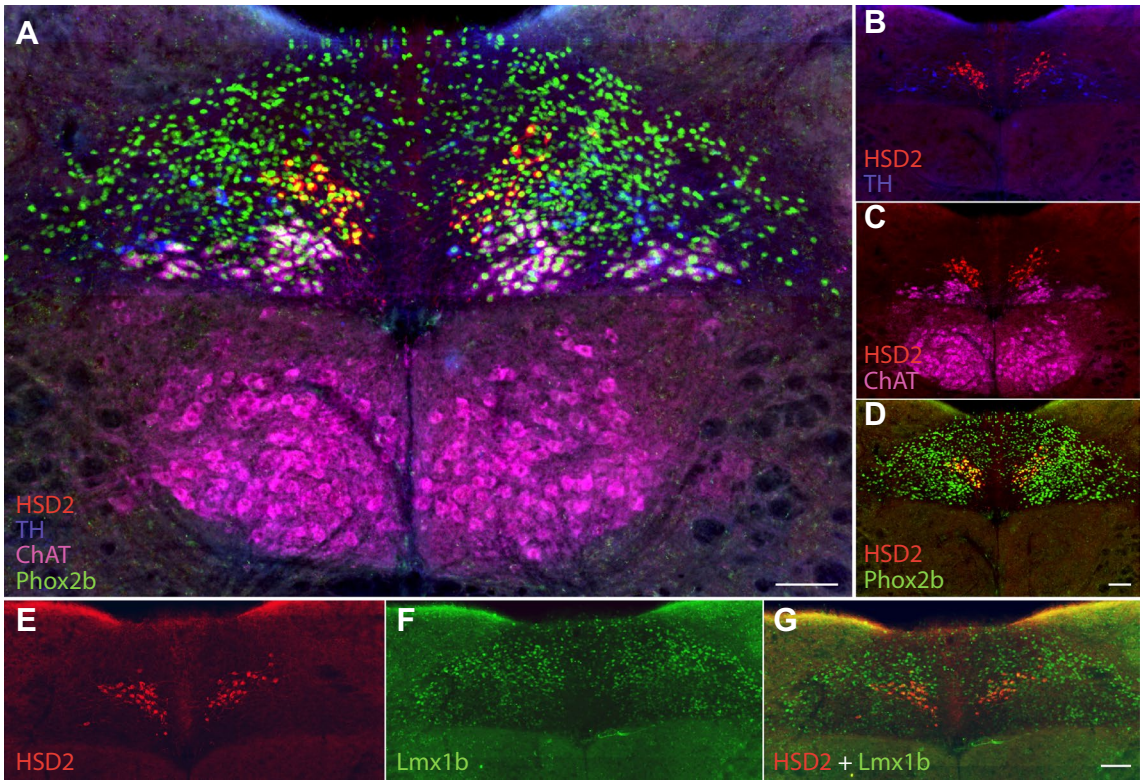

Fig. 2 **a** HSD2-immunoreactive neurons (red) contain nuclear immunoreactivity for the transcription factor Phox2b (green; double-labeling is yellow). HSD2 neurons are separate from Phox2b neuron populations labeled for tyrosine hydroxylase (TH, blue) and choline acetyltransferase (ChAT, magenta). **b–d** Compare each pair of markers. **e–g** Nuclear immunoreactivity for Lmx1b (green) is present in many HSD2 neurons and other neurons across the dorsal NTS. Scale bars are 100 µm and apply to adjoining panels of similar size

area postrema (Fig. 1c). From there, sparse HSD2 neurons extend through the caudal commissural NTS back to the pyramidal decussation, which marks the spinomedullary transition (Fig. 1d). Across all counted cases in this study, this population includes on average 116 ± 16 immunoreactive neurons per mouse (Abercrombie-corrected counts from $n = 25$ male mice), which is approximately one-fifth their number in rats (~ 600; Geerling et al. 2006b), but can range from as few as 48 to as many as 326 per mouse. Estimating this NTS population from neuronal expression of *Hsd11b2* mRNA yields a slightly lower estimate, 98 ± 7 per mouse ($n = 18$, range 51–167).

As in rats, HSD2-immunoreactive neurons contain strong nuclear immunoreactivity for Phox2b (100% of HSD2 neurons in $n = 3$ cases), which is a transcription factor marker of cholinergic and glutamatergic principal neurons in the dorsal vagal complex (Kang et al. 2007; Geerling et al. 2008). HSD2 neurons are distinct from other Phox2b-expressing neurons in the dorsal vagal complex, including A2 and C2d catecholaminergic NTS neurons, which are immunoreactive for tyrosine hydroxylase (TH; Fig. 2b) and cholinergic neurons, which are immunoreactive for choline acetyltransferase (ChAT; Fig. 2c). HSD2 neurons also lack immunoreactivity for the nuclear transcription factor FoxP2 (not shown), which identifies their target neurons in the parabrachial complex (Geerling et al. 2011), but is found only outside the NTS in tissue sections containing HSD2 neurons, with sparse nuclear labeling in the reticular formation and dense labeling throughout the inferior olivary nucleus. Many dorsal HSD2 neurons contain nuclear immunoreactivity for the nuclear transcription factor Lmx1b (31 ± 4%, $n = 4$; Fig. 2e–g), which is found in many other dorsal NTS neurons and extends laterally and caudally into the outer layers of the spinal trigeminal nucleus and dorsal horn of the spinal cord (Szabo et al. 2015).

Outside the NTS, no other brain region contains HSD2-immunoreactive cells (Supplementary Figure A1), as reported previously for *Hsd11b2* expression in adult mice (Holmes et al. 2006). Specifically, and in contrast to some reports in rats (Robson et al. 1998; Haque et al. 2015), we do not find any HSD2-immunoreactivity above background levels in the paraventricular hypothalamic nucleus, supraoptic hypothalamic nucleus, or amygdala (Supplementary Figure A2). Even in regions with HSD2-immunoreactive cells in rats—the subcommissural organ and ventrolateral subdivision of the ventromedial

hypothalamic nucleus (Roland et al. 1995; Geerling et al. 2006b; Geerling and Loewy 2009)—we do not find any HSD2 immunoreactivity in mice (Supplementary Figure A2).

Thus, every adult mouse brain contains a robust distribution of *Hsd11b2*-expressing, HSD2-immunoreactive neurons, exclusively in the NTS. Their distribution lacks the dense, rostral cluster found in rats and is roughly one-fifth the size, but is otherwise similar to the homologous population of HSD2 neurons in rats.

HSD2 neurons occupy a BBB-deficient zone

Immediately ventral to the area postrema, the medial NTS subdivision has an incomplete blood–brain barrier (BBB). A gradient exists between the area postrema, a circumventricular organ with fenestrated capillaries, and the rest of the brainstem. This gradient extends ventrally and laterally through much of the medial NTS (Gross et al. 1990; Broadwell and Sofroniew 1993; Geerling and Loewy 2009).

To learn whether HSD2 neurons lie inside this zone of enhanced BBB permeability, we injected Fluorogold i.p. (hydroxystilbamidine; $n=3$), which enters the vasculature and produces intraluminal labeling in blood vessels throughout the brain, plus retrograde axonal labeling of neurons that extend axons outside the BBB, and pertinent to this study, extracellular labeling in regions lacking a BBB. In the dorsal vagal complex, Fluorogold intensely labels the area postrema neuropil and retrograde labels all cholinergic neurons in the dorsal vagal and hypoglossal motor nuclei (Fig. 3a–d). It also produced extensive, extracellular labeling in the subpostremal NTS with a gradient of intermediate intensity between the area postrema and BBB-protected regions of the medulla. No HSD2-immunoreactive neurons contained intracellular Fluorogold, confirming that they do not extend axons outside the BBB, yet many HSD2 dendrites and cell bodies lie within the zone of intermediate extracellular Fluorogold labeling (Fig. 3a). This relationship is more prominent at rostral and middle levels of the HSD2 distribution then tapers caudally; the commissural NTS did not contain any Fluorogold.

To also assess whether endogenous, circulating macromolecules can access this brainstem region, we immunolabeled mouse immunoglobulin G (IgG), a family of large proteins that cannot penetrate the BBB (Broadwell and Sofroniew 1993). Consistently in C57B6/J mice ($n=3$), immunolabeling for IgG was prominent in the area postrema and even more prominent in a gradient through the subpostremal NTS, nearing or surrounding many HSD2 neurons and their dendrites (Fig. 3e–h).

Genes expressed by HSD2 neurons

To first verify that HSD2 immunoreactivity is specific to neurons expressing *Hsd11b2*, we performed fluorescence in situ hybridization (FISH) for this transcript followed by immunofluorescence labeling for HSD2 protein in the same tissue sections. With a strict criterion of at least ten distinct mRNA transcripts per cell, *Hsd11b2* mRNA co-localized in 93 ± 1 HSD2-immunoreactive neurons (and only in these neurons; range 91–94%, $n=3$), confirming the specificity of the rabbit anti-HSD2 antiserum (Fig. 4a–c).

We next combined labeling for HSD2 or *Hsd11b2* with FISH for markers previously identified using single-cell RNA-seq in mice (Resch et al. 2017) or immunolabeling in rats (Geerling et al. 2006b, 2008). We confirmed that all HSD2 neurons express mRNA for *Phox2b* ($100\pm0\%$, $n=3$), which occupies the same NTS neuronal distribution as Phox2b-immunolabeled nuclei (Fig. 4d–f). All HSD2 neurons also express the type 2 vesicular glutamate transporter (Vglut2/*Slc17a6*; $100\pm0\%$, $n=3$; Fig. 4g–i), which complements evidence for Fos activation in their efferent target neurons when HSD2 neurons are active (Geerling and Loewy 2007c; Geerling et al. 2011; Jarvie and Palmiter 2017) and for synaptic glutamate release by their axon terminals in the same sites (Resch et al. 2017).

Next, having co-localized mineralocorticoid receptor (MR) immunolabeling with HSD2 in rats (Geerling et al. 2006b) and complementing RNA-seq data in mice (Resch et al. 2017), we examined mRNA co-localization with *Nr3c2* and found mRNA for this receptor in all *Hsd11b2*-expressing neurons in the NTS ($100\pm0\%$, $n=3$; Fig. 4j–l). MR expression was most prominent in HSD2 neurons, but unlike *Hsd11b2*, we also found light *Nr3c2* mRNA in a minority of NTS neurons outside their distribution, and in hypoglossal motor neurons and in other brain regions, most prominently the hippocampus, similar to a previous report in the rat brain (Arriza et al. 1988).

GFP BAC-transgenic mice for the angiotensin II receptor (*Agt1ar*-GFP) have an NTS cluster of GFP-expressing cells resembling the HSD2 neuron distribution (Gonzalez et al. 2012). Overall, $60\pm2\%$ of HSD2-immunoreactive neurons expressed GFP in these mice (range 56–63%; Fig. 4m–o). To re-examine the assertion that all NTS neurons with *Agt1ar*-GFP are catecholaminergic (Gonzalez et al. 2012), we then immunolabeled HSD2 together with the catecholamine neuron marker, TH, and find that each marker accounts for a distinct, similar proportion of *Agt1ar*-GFP + neurons in the NTS ($19\pm1\%$, HSD2; $20\pm0\%$, TH; $n=2$); as above, no neurons contained HSD2 and TH. As BAC-transgene expression is sometimes ectopic relative to endogenous gene expression, we also assessed the expression of endogenous *Agtr1a* and found that $97\pm2\%$ of *Hsd11b2*-expressing neurons also contain mRNA for *Agtr1a*, the angiotensin II receptor

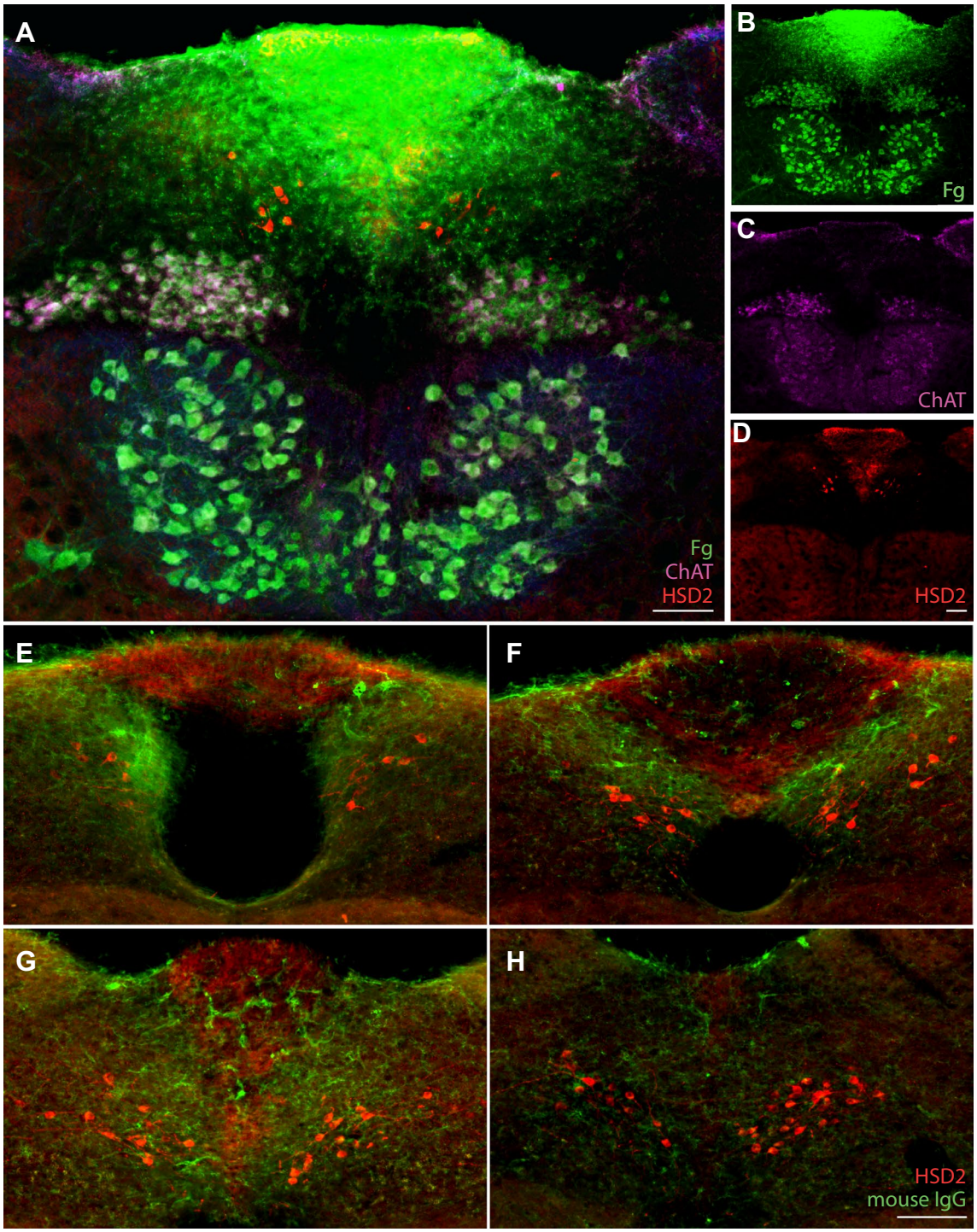

Fig. 3 **a–d** After systemic injection, Fluorogold (Fg, green) permeates the area postrema (AP) and the adjacent NTS, up to and including the distribution of HSD2-immunoreactive neurons (red). Retrograde Fg transport in peripheral axons also labels ChAT-immunoreactive (magenta) neurons in the dorsal vagal and hypoglossal motor nuclei. Scale bars are 100 µm. **e–h** Immunoglobulin G (IgG) immunofluorescence highlights linear structures in the area postrema and a large subpostremal region of the NTS up to and around many HSD2-immunolabeled (red) neurons particularly at the obex (**a**) and tail of the area postrema (**g**). Scale bar is 100 µm

(Fig. 4p–r). In contrast, mRNA for angiotensinogen (*Agt*, the precursor for angiotensin peptides), though abundant in the dorsal vagal complex, co-localizes exclusively with the astrocytic gene *Apoe*, never *Hsd11b2* or *Phox2b* (not shown), consistent with evidence that brain *Agt* expression is astrocyte-specific (Stornetta et al. 1988; Zeisel et al. 2018).

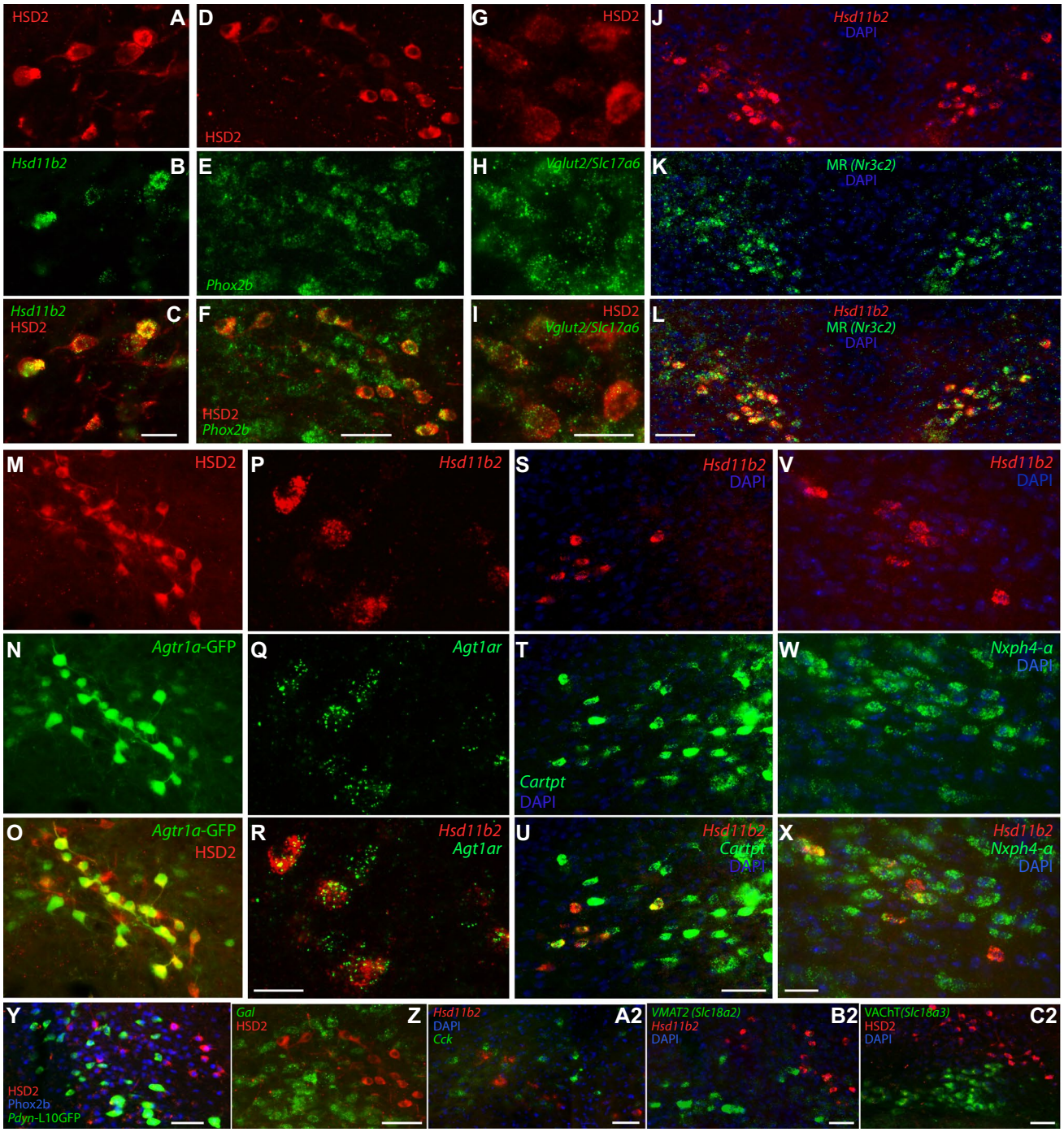

After searching the literature and Allen Brain Atlas for candidate markers, we identified two neuropeptide mRNAs that are expressed in HSD2 neurons. *Cartpt* (cocaine- and amphetamine-regulated transcript, Fig. 4s–u) co-localized in half (50 ± 4%; $n = 3$) and *Nxph4* in virtually all (96 ± 1%; $n = 3$) of *Hsd11b2*-expressing neurons (Fig. 4v–x). HSD2 neurons do not express a Cre-reporter for dynorphin in *Pdyn-IRES-Cre;R26-lsl-L10GFP* mice ($n = 2$; Fig. 4y), in which we separately verified co-localization between GFP and endogenous *Pdyn* mRNA expression (not shown). *Pdyn* L10GFP + neurons in the NTS do contain Phox2b-immunoreactive nuclei similar to HSD2 and other glutamatergic NTS neurons, and are densest at intermediate levels of the NTS (rostral and lateral to the HSD2 neurons) with several others in the dorsal vagal motor nucleus. In contrast to our finding about small numbers of HSD2 neurons with galanin immunoreactivity in rats (Geerling et al. 2006b), none from the large, prominent population of medial NTS neurons

◂**Fig. 4** A variety of gene expression in the NTS distinguishes HSD2 and surrounding neurons, evidence by fluorescence in situ hybridization (FISH), immunofluorescence, and GFP reporter expression. **a–c** HSD2 immunoreactivity (red) and *Hsd11b2* mRNA (green) co-localize in the same NTS population. **d–f** Complementing their Phox2b immunoreactivity in Fig. 2, all HSD2-immunoreactive neurons and many dorsal vagal complex neurons, contain *Phox2b* mRNA (green). **g–f** Along with many other neurons in the NTS and elsewhere, all HSD2 neurons contain mRNA for the type 2 vesicular glutamate transporter (Vglut2/*Slc17a6*, green). **j, k** Mineralocorticoid receptor mRNA (*Nr3c2*, green) is expressed prominently in NTS neurons that contain mRNA for *Hsd11b2* (red). **m–o** BAC-transgenic mice expressing GFP following the angiotensin II receptor gene (*Agtr1a*-GFP) have a prominent cluster of green neurons in the NTS, many of which are immunoreactive for HSD2 (red). **p–r** We confirmed in C57BL6/J mice that mRNA for this receptor (*Agtr1a*, green) is expressed in a similar pattern in the medial NTS, and co-localizes with mRNA for *Hsd11b2* (red). **s–x** HSD2 neurons (*Hsd11b2* mRNA, red) co-localize with many cells from larger NTS populations expressing the neuropeptide precursors *Cartpt* (green, **t, u**) and *Nxph4* (green, **w, x**). HSD2 neurons do not express a variety of other neuropeptide genes or Cre-reporters, including the L10GFP Cre-reporter for *Pdyn* (**y** note that the putative *Pdyn* NTS neurons are immunoreactive for Phox2b, blue) or mRNA for galanin (*Gal*, green **z**), or cholecystokinin (Cck, green, **a2**). Complementing their lack of catecholaminergic and cholinergic synthetic enzyme markers in HSD2 neurons in Fig. 2, Hsd11b2 does not co-localize with mRNA for the vesicular monoamine transporter 2 (VMAT2/*Slc18a2*, green in **b2**) or vesicular acetylcholine transporter (VAChT/*Slc18a3*, green in **c2**). Scale bars are 20 µm (**a**), 25 µm (**f, i, r** and **x**) and 50 µm (**l, o, r, u, y, z, a2, b2, c2**) and apply to adjoining panels of similar size

expressing *Gal* mRNA express *Hsd11b2* ($n=3$; Fig. 4z). *Cck* (cholecystokinin) mRNA in many neighboring and intermingled NTS neurons was found in just $2 \pm 1\%$ of Hsd11b2-expressing NTS neurons (range 0–3%, $n=3$; Fig. 4a2). Also, consistent with their lack of immunoreactivity for ChAT and TH, *Hsd11b2*-expressing neurons did not contain detectable mRNA expression for synaptic vesicle transporters for acetylcholine (*Slc18a3;* $n=1$) or monoamines (*Slc18a2;* $n=1$) (Fig. 4b2–c2).

Fate-mapping *Hsd11b2* using Cre-reporters

To identify cells with a developmental history of *Hsd11b2* expression (or that derive from a cell lineage that expressed *Hsd11b2*), we examined Cre-reporter expression in adult offspring from two different strains of knockin Cre mice—*Hsd11b2-Cre* (Naray-Fejes-Toth and Fejes-Toth 2007) or *Hsd11b2*^{Cre} (Jarvie and Palmiter 2017)—crossed with one of three different strains of fluorescent Cre-reporter mice with lox-STOP-lox fluorescent proteins in the ROSA26 locus. Corresponding to the variable efficiency of various Cre-reporter strains, these combinations yielded more and more consistent patterns of fluorescent protein expression, as follows.

Hsd11b2-Cre;R26-LSL-L10GFP mice express L10GFP prominently in the cerebellar granule cell layer (Fig. 5a). This is consistent with the initial report of a beta-galactosidase reporter for this Cre strain (Naray-Fejes-Toth and Fejes-Toth 2007), and is expected from reports of abundant *Hsd11b2* expression by proliferating granule cells in the late-embryonic and early-postnatal period (Diaz et al. 1998; Robson et al. 1998; Holmes et al. 2006). In the NTS, despite a normal distribution of HSD2-immunoreactive neurons, we found GFP in just few neurons in most mice. One mouse had zero HSD2 neurons with GFP (Fig. 5b), despite abundant GFP expression in cerebellar granule cells, similar to littermates. In the remaining L10GFP reporter mice ($n=7$), at most one or a few HSD2 neurons contained GFP per section (Fig. 5c), reflecting a low efficiency of this particular Cre-driver/reporter combination. Several other brain regions had sparse GFP, but the regions and cell distributions were inconsistent between littermates, and often differed between the right and left sides of the brain.

Due to the sparse and inconsistent L10GFP reporter performance, we next crossed *Hsd11b2-Cre* mice to the Ai9 tdTomato strain (Madisen et al. 2010). The resulting *Hsd11b2-Cre;(Ai9)R26-LSL-tdTomato* mice express tdTomato robustly in the cerebellum, filling the soma and processes of all granule cells (Fig. 5d). In contrast to L10GFP, every Ai9 mouse expressed tdTomato in a majority of HSD2 neurons (Fig. 5e). We also see tdTomato in a wider variety of cell types across virtually every brain region. Several regions contain individual neurons, clusters of neurons, or bundles of axon, but most tdTomato-positive cells have non-neuronal morphologies. Some appear to wrap processes around blood vessels (Fig. 5f) and others, scattered in white matter tracts, extend two or three long, thin processes in an appearance similar to oligodendrocyte precursor cells (Fig. 5g).

Due to the divergent expression patterns between these two reporter strains, we chose to examine a third Cre-driver/reporter combination. We crossed a different Cre-driver strain, *Hsd11b2*^{Cre} (Jarvie and Palmiter 2017) to the Ai75 Cre-reporter with nuclear-localized tdTomato. These *Hsd11b2*^{Cre}; *(Ai75)R26-LSL-NLStdTomato* mice express nuclear tdTomato throughout the cerebellar granule cell layer (Fig. 5H). We examined sections through the full brain in five cases and found intense nuclear tdTomato expression in diverse cell types at every level of the brain (Supplemental Figure A3). This distribution was similar to, but more uniform than the Ai9 reporter above, with consistently prominent tdTomato expression throughout the pontine nuclei and thalamus atop a more uniform population scattered evenly across the neuroaxis. In these same brains, despite the abundance of Cre-reporter expression, no region outside the NTS contained any HSD2-immunoreactive cells. We confirmed this using NiDAB immunohistochemistry for maximum sensitivity and as in C57B6/J mice, we did not find HSD2-immunoreactive cells in any region except the NTS (Supplemental Figures A1, A2).

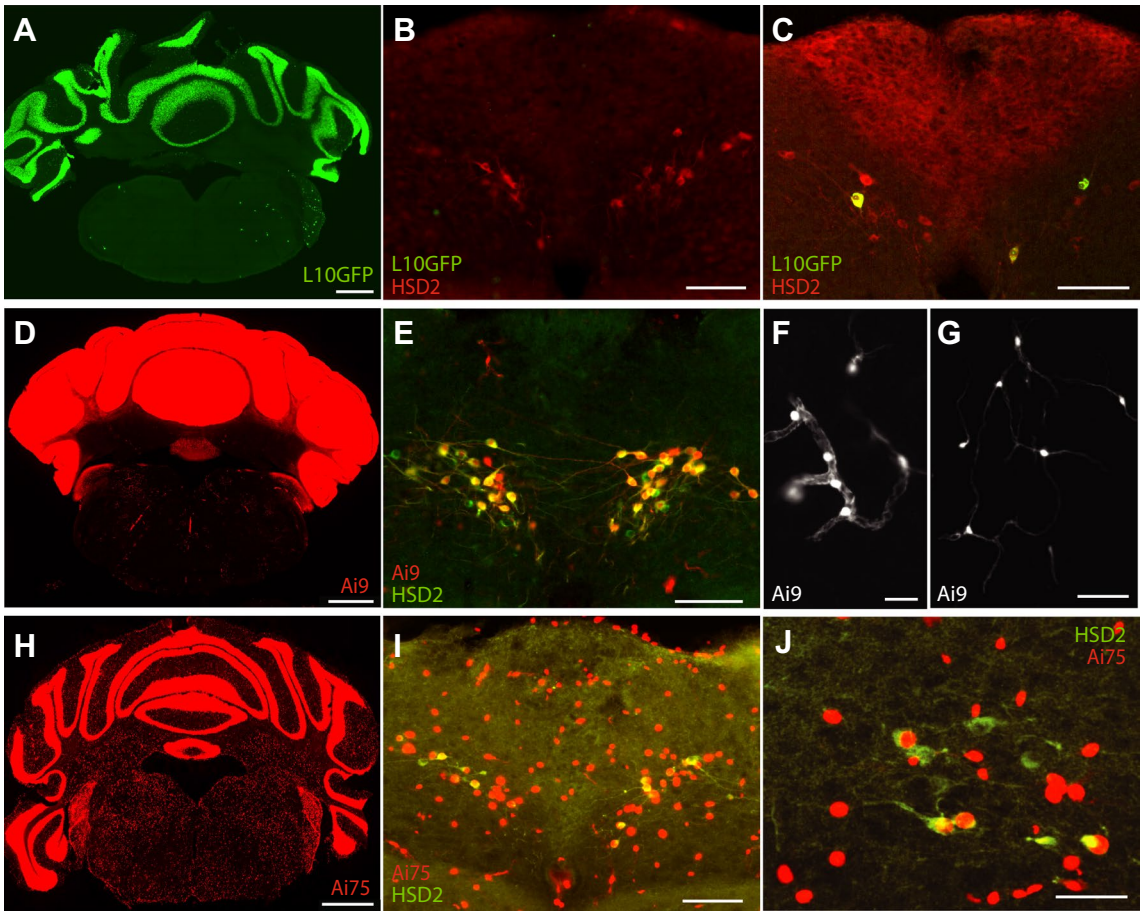

Fig. 5 *Hsd11b2* Cre-driver mice crossed to separate strains of Cre-reporter mice: **a–c** *Hsd11b2-Cre;R26-lsl-L10GFP*, **d–g** *Hsd11b2-Cre;R26-lsl-Ai9tdTomato*, and **h–j** *Hsd11b2*^{Cre}*;R26-lsl-Ai75tdTomato*. **a, d, h** The cerebellum exhibits similar Cre-reporter expression in all three strains, with differences related to the expected intrcellular distribution of each fluorescent protein: L10GFP is tethered to ribosomes in cytoplasm; Ai9 tdTomato diffuses freely into dendrites and axons; and Ai75 tdTomato is targeted to the cell nucleus. In the NTS, the L10GFP reporter was sparse, with **b** one mouse expressing no GFP in any HSD2 neurons and **c** others containing a most one or few GFP-expressing HSD2 neurons per tissue section. The Ai9 reporter was expressed in virtually all HSD2 neurons (**e**) and many other cell types, including clusters of smalls cells and processes surrounding blood vessels (**f**) and small glial cells that appear similar to oligodendrocyte precursor cells (**g**). The Ai75 reporter filled the cell nucleus with intensely bright fluorescence in many cell types throughout the brain, including most HSD2 neurons (**i**), which in some cases were fewer in number and abnormal in appearance (see text). Scale bars are 1 mm (**a, d, h**) and 100 µm (all other panels)

In the NTS, most HSD2 neurons contained nuclear tdTomato (Fig. 5i). However, the first two brains we examined had very few HSD2-immunoreactive neurons in the NTS (13 and 16 total HSD2 neurons). These neurons appeared dysmorphic, with faint HSD2-immunoreactivity, suggesting that the abundant tdtomato in their nuclei exerts a toxic effect. We sodium-depleted two reporter mice to boost HSD2 expression (Geerling and Loewy 2006c, 2007c); one had light HSD2-immunoreactivity in a moderate number of HSD2 neurons (44; Fig. 5j), while the other had a normal number (69) of normal-appearing HSD2-immunoreactive neurons. We later found three mice from this strain that had survived to 22 weeks, and again immunolabeled HSD2. Two of these mice had zero HSD2-immunoreactive neurons, and one mouse had just two HSD2-immunoreactive neurons in the NTS, neither of which contained nuclear tdtomato; a Cre-negative littermate, simultaneously perfused and immunolabeled as a positive control, had a normal distribution of HSD2 neurons in the NTS. In sum, the Ai75 nuclear tdTomato reporter appears to have a chronic, toxic effect on HSD2 neurons. Most *Hsd11b2*^{Cre}*;(Ai75)R26-LSL-NLStdTomato* mice were underweight, with few surviving past 6–7 weeks of age, further suggesting a toxic effect of Ai75 nuclear tdTomato,[1] so we euthanized this strain.

[1] In preparing this manuscript, we also found evidence of Ai75 neurotoxicity in *Slc17a7-IRES3-Cre* mice (http://connectivity.brain-map.org/transgenic/experiment/304698566), which appears to be age-related and specific to regions that express that Cre-driver gene (hippocampus, cerebral cortex).

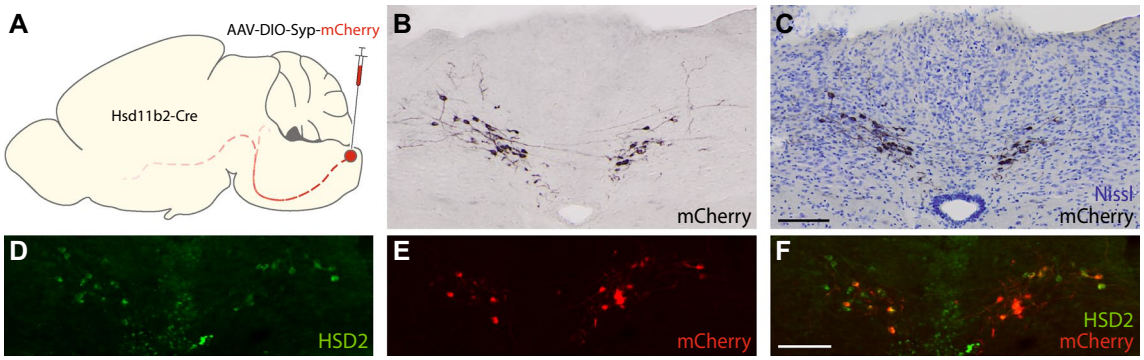

Fig. 6 Experimental strategy for Cre-conditional labeling axonal projections from HSD2 neurons in the NTS to other brain regions (**a**). **b–f** A representative injection site from the cases we hand-traced to show the brain-wide pattern of axonal labeling in Fig. 7 (with detail images in Supplemental Figure A4). **b** Nickel-DAB immunohistochemistry (black, NiDAB) reveals mCherry expression by Cre-expressing neurons within the injected region. **c** Nissl-counterstained and reimaged image of the same tissue section clarifies background cytoarchitecture. **d–f** Cre-conditional expression of Syp-mCherry (red) co-localizes with HSD2-immunofluorescence (green) in a section adjacent to the NiDAB-stained NTS section shown in **b, c**. Scale bars are 100 µm and apply to adjoining panels of similar size

Cre-dependent axon labeling

Next, to label the axonal projections of HSD2 neurons, we delivered Cre-conditional ChR2-mCherry ($n=3$) or Syp-mCherry ($n=4$) into the NTS of *Hsd11b2-Cre* mice, and Syp-mCherry in *Hsd11b2*^{Cre} mice ($n=4$). Both ChR2-mCherry and Syp-mCherry label axons, but ChR2 inserts into the cell membrane along the length of the axon, while Syp concentrates preferentially in synaptic boutons. Despite large injection volumes of 90–200 nL bilaterally, with each AAV injection spreading presumably through a large extent of the dorsal vagal complex and beyond, we did not find mCherry-expressing neurons outside the NTS in any of these cases. ChR2-mCherry and Syp-mCherry cases did not differ in their patterns of neuron and axonal labeling except, as expected, the synaptophysin conjugate accumulates more in boutons (terminal and en passant), while the channelrhodopsin conjugate more evenly labels axonal shafts and boutons. We reviewed axonal labeling in all 3 ChR2-mCherry cases, but focused our subsequent analysis on Syp-mCherry due to the enriched bouton labeling.

Figure 6 shows Cre-conditional Syp-mCherry expression in the NTS of a *Hsd11b2-Cre* mouse. In these cases ($n=4$ and $n=4$, separate strains of *Hsd11b2* Cre-driver mice), the percentage of HSD2-immunreactive neurons expressing Syp-mCherry ranged from 21 to 84% (mean 46 ± 9%). Expression was specific to the HSD2 population, as on average 97 ± 1% of neurons expressing Syp-mCherry were immunoreactive for HSD2 (range 0–9%). In some mice, the distribution of labeled neurons skewed somewhat rostrally or caudally, or more to the left or right side of the NTS, but in combination our cases covered the full, bilateral HSD2 neuron distribution at all rostrocaudal levels. More axons are apparent in cases with more HSD2 neurons expressing Syp-mCherry, but the overall pattern of brain regions receiving axons was the same in all cases. In two cases expressing Syp-mCherry labeling on one side of the NTS, axonal projections remained predominantly ipsilateral throughout the brainstem and forebrain and we did not observe any commissural axons (axons crossing from one side of the brain to the other) in any brain at any level, indicating that axonal projections of HSD2 neurons are largely ipsilateral.

We traced the full, rostrocaudal distribution of axons emerging from the NTS in a mouse with 79% of HSD2 neurons expressing Syp-mCherry (Fig. 6d–f), using Ni-DAB immunohistochemistry to label mCherry with maximum sensitivity and Nissl counterstaining to help identify brain regions labeled in Fig. 7. Brightfield photomicrographs in Supplemental Fig. 4 supplement these drawings, along with immunofluorescence and mRNA labeling in major target sites (Figs. 8, 9).

Labeled axons project laterally from the NTS into the medullary reticular formation (Fig. 7a, b). They do not arborize and do not appear to form boutons within the NTS, nor do they arborize extensively in the reticular formation. Instead, they course rostrally through it (Fig. 7c–l), remaining dorsal to the ventrolateral medullary region that contains cardiorespiratory, vagal, and other visceromotor neurons. Specifically, the nucleus ambiguus, the ventral respiratory column, and lateral paragigantocellularis nucleus of the rostral and caudal ventrolateral medulla (RVLM/CVLM) were devoid of axonal labeling in every case, in both Cre-driver strains, and with both axonal tracers.

Labeled axons continue rostrally, over the facial motor (VII) nucleus and past the exiting VII nerve fascicles (Fig. 7g–i), then turn dorsally, abruptly beneath the motor nucleus of the trigeminal nerve (Vmo) and course past its motoneurons (Fig. 7j–m). After continuing dorsally past

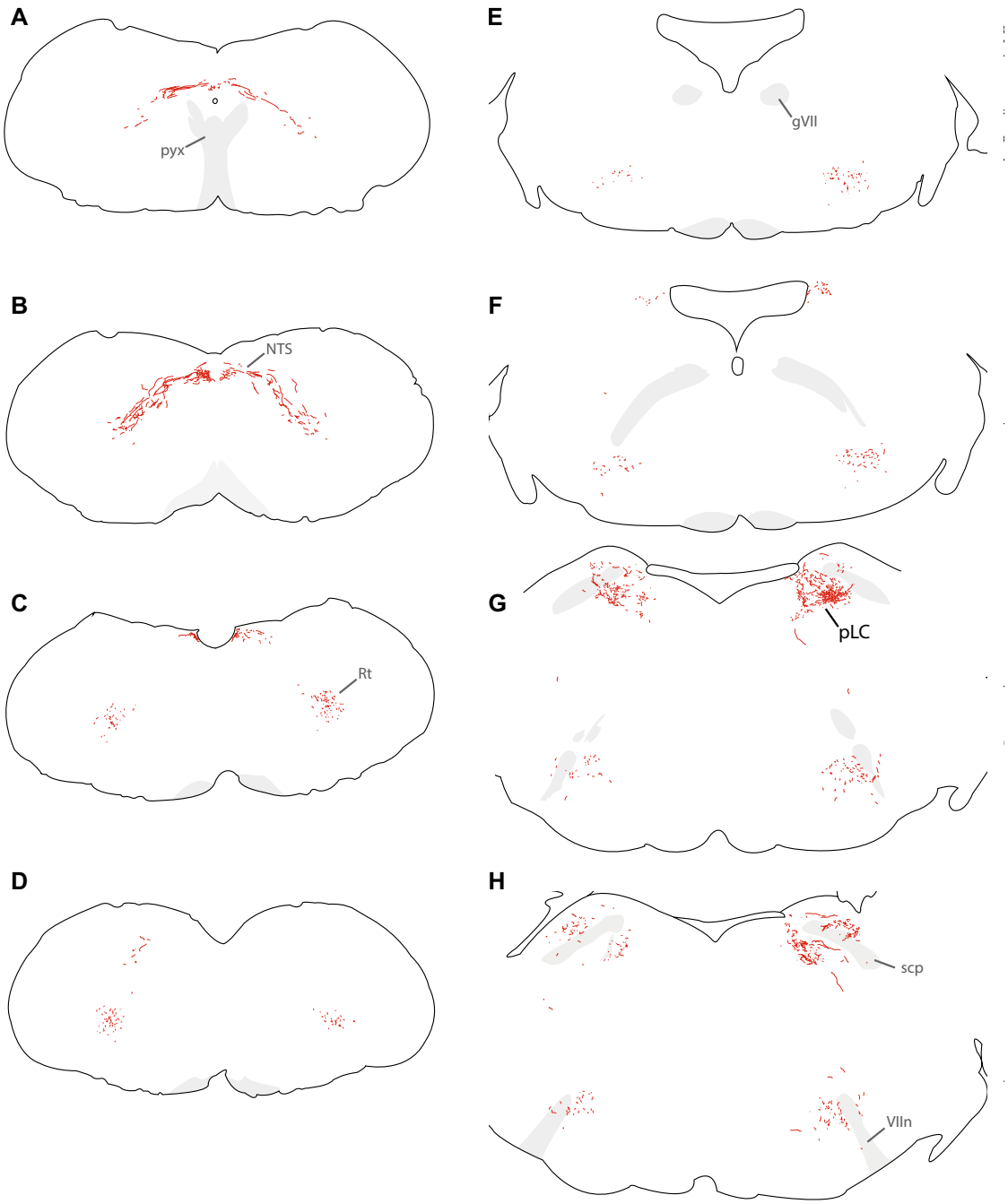

Fig. 7 We traced axonal projections of HSD2 neurons in a representative *Hsd11b2-Cre* mouse injected with Cre-conditional Syp-mCherry (injection site in Fig. 6). These successive, caudal-to-rostral tracings show the full-brain distribution of Syp-mCh axons in this case. Each drawing was re-scaled for illustrative purposes, and a minimal set of labels are provided to highlight relevant landmarks, pathways, and target regions. *ac* anterior commissure, *BSTvL* ventrolateral subregion of the bed nucleus of the stria terminalis, *fx* fornix, *gVII* genu of the seventh cranial nerve fascicles, *mCeA* medial subdivision of the central nucleus of the amygdala, *ml* medial lemniscus, *NTS* nucleus of the solitary tract, *PAGvL* ventrolateral subdivision/column of the periaqueductal gray matter, *PBcL* central lateral parabrachial subnucleus, *pLC* pre-locus coeruleus, *PSTN* parasubthalamic nucleus, *pyx* pyramidal decussation, *Rt* medullary (intermediate) reticular formation, *scp* superior cerebellar peduncle, *sLHA* suprafornical lateral hypothalamic area, *VIIn* seventh cranial nerve root, *xscp* decussation of the superior cerebellar peduncle

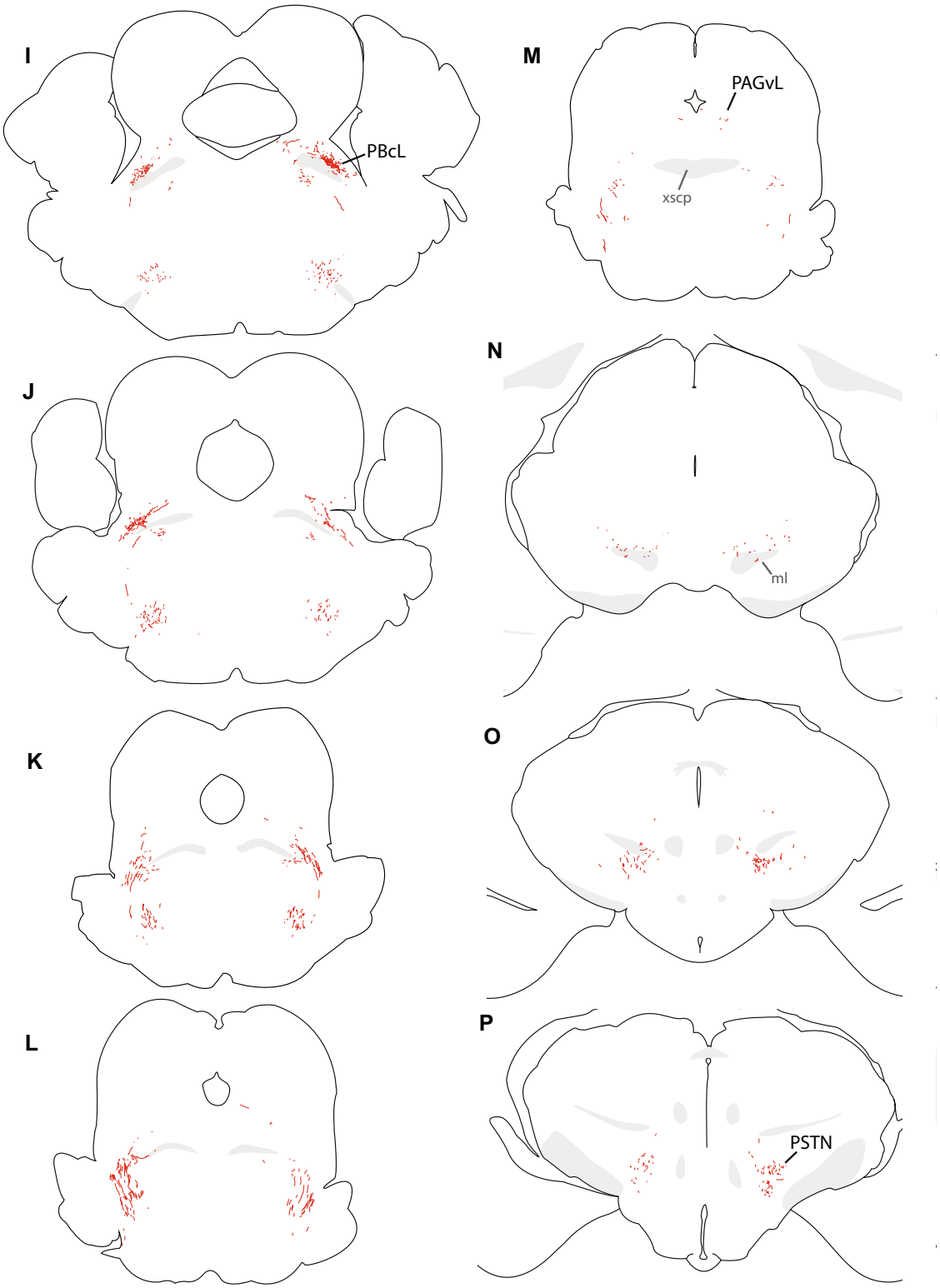

Fig. 7 (continued)

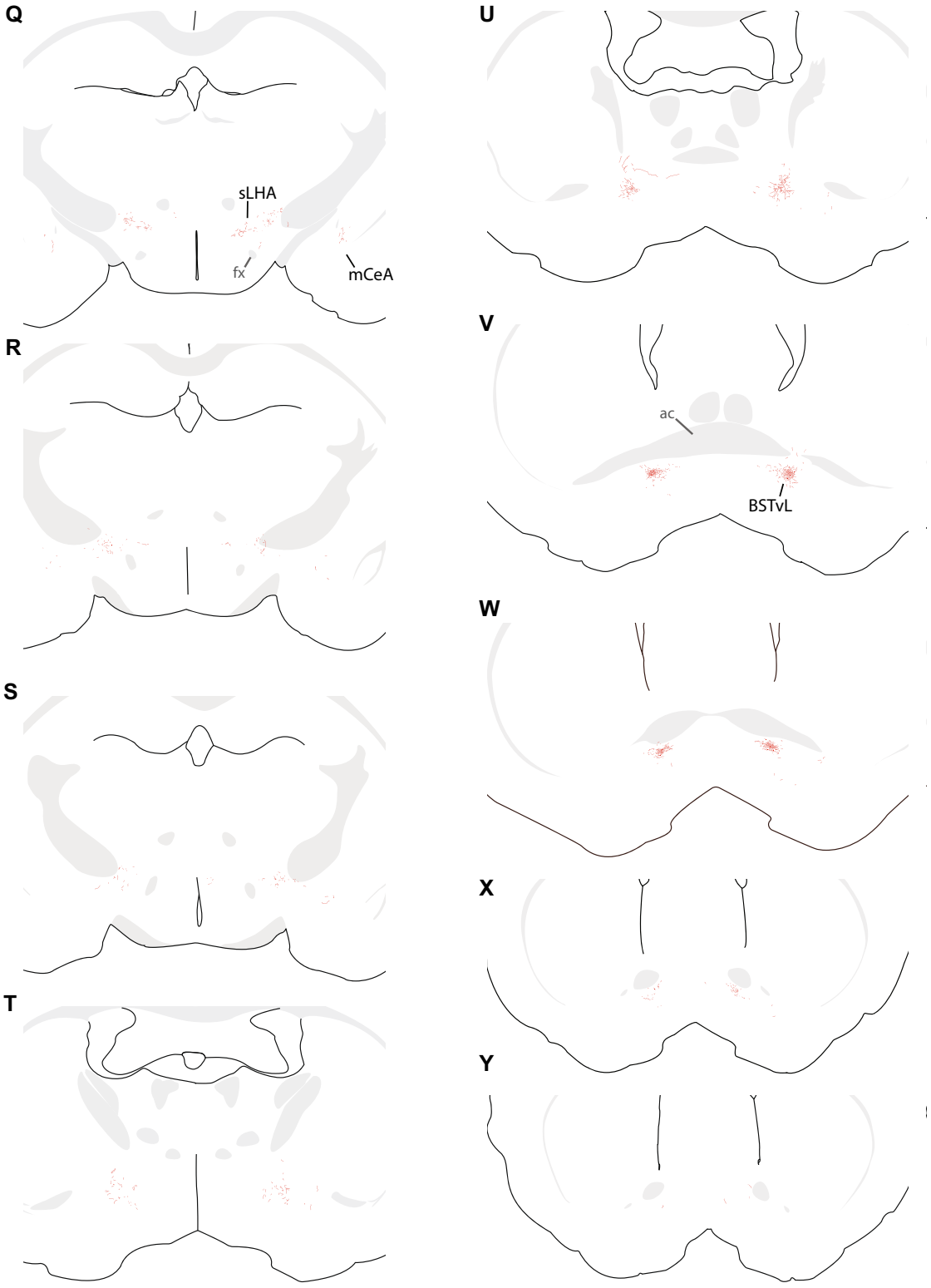

Fig. 7 (continued)

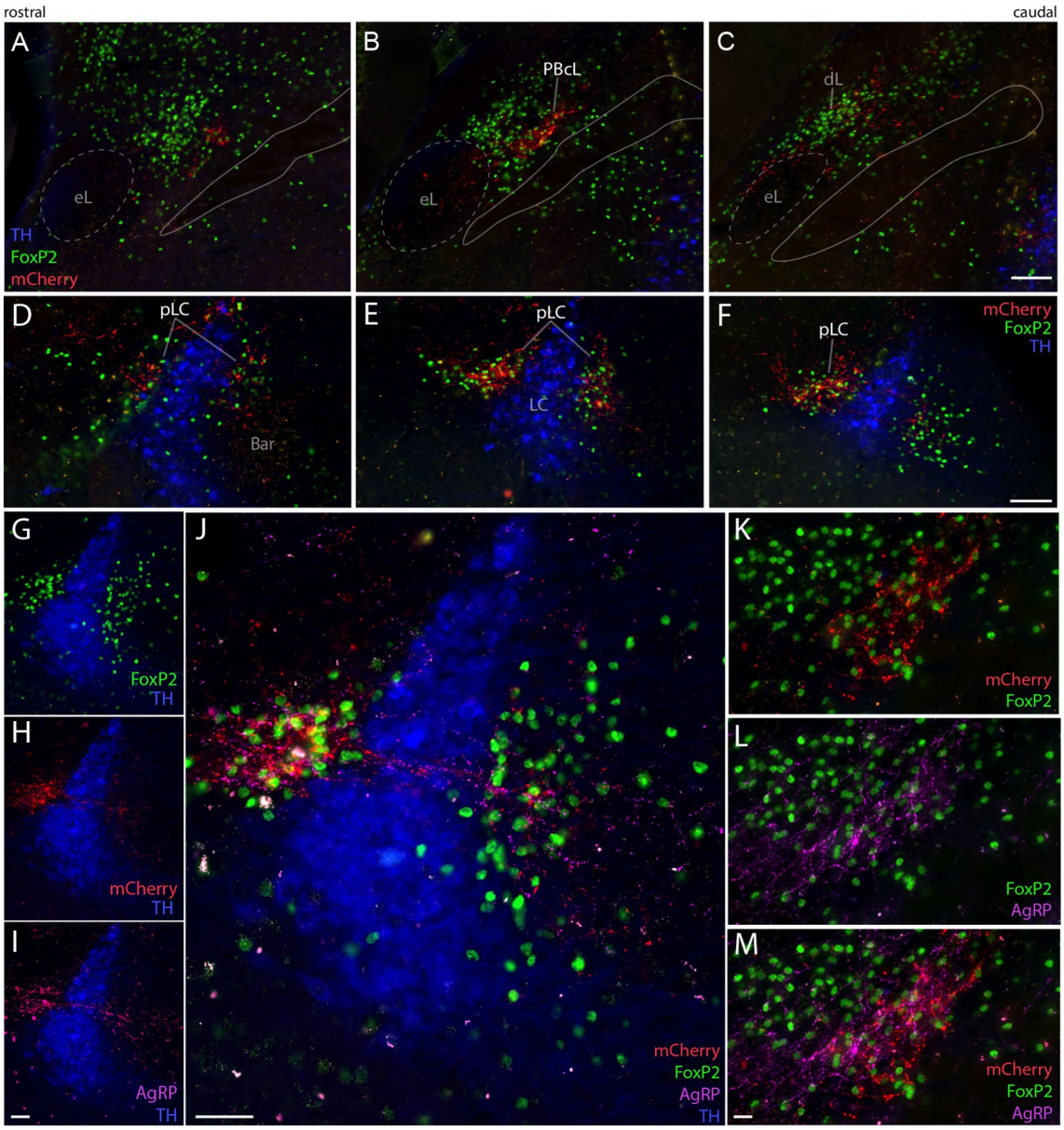

Fig. 8 HSD2 neurons project axons that terminate densely (red, mCherry) in a highly specific subregion of the parabrachial complex (PB), in close association with other axons containing the neuropeptide AgRP (agouti-related peptide, magenta). We labeled a transcription factor marker (green, FoxP2-immunoreactivity) and catecholamine neuron marker for locus coeruleus (LC; immunoreactivity in blue for tyrosine hydroxylase, TH) for reference in this crowded, complex region of the brainstem. **a**–**c** HSD2 axons in the lateral PB terminate densely amid FoxP2 neurons within a narrow subregion of the PB central lateral subnucleus (PBcL), with minimal labeling in its dorsal lateral (dL) and external lateral (eL). **d**–**f** Caudally, HSD2 axons target the pre-locus coeruleus (pLC) FoxP2 neuron cluster flanking and streaking through the LC, while largely avoiding Barrington's nucleus (Bar, **d**) and the most caudal–medial extent of FoxP2 neurons in this region (**f**). In both pLC (**g**–**j**) and PBcL (**k**–**m**), the axon-terminal field of HSD2 axons is closely associated with a dense collection of axons and boutons immunoreactive for AgRP. All scale bars are 100 µm

Vmo, many axons turn caudally to reach the parabrachial (PB) complex at the hindbrain–midbrain junction, just ventral to the isthmus of the inferior colliculus. As they progress caudally through the lateral PB, these axons arborize in discrete subregions. First, they form a dense, thin terminal field in a subregion of the central lateral PB subnucleus (PBcL) near the superior cerebellar peduncle (Fig. 8a–c). At the fringes of this terminal field are sparser branches and boutons in the PB external lateral and dorsal lateral subnuclei.

From there, labeled axons continue caudally and medially, branching extensively and streaking beneath the superior cerebellar peduncle and through the mesencephalic

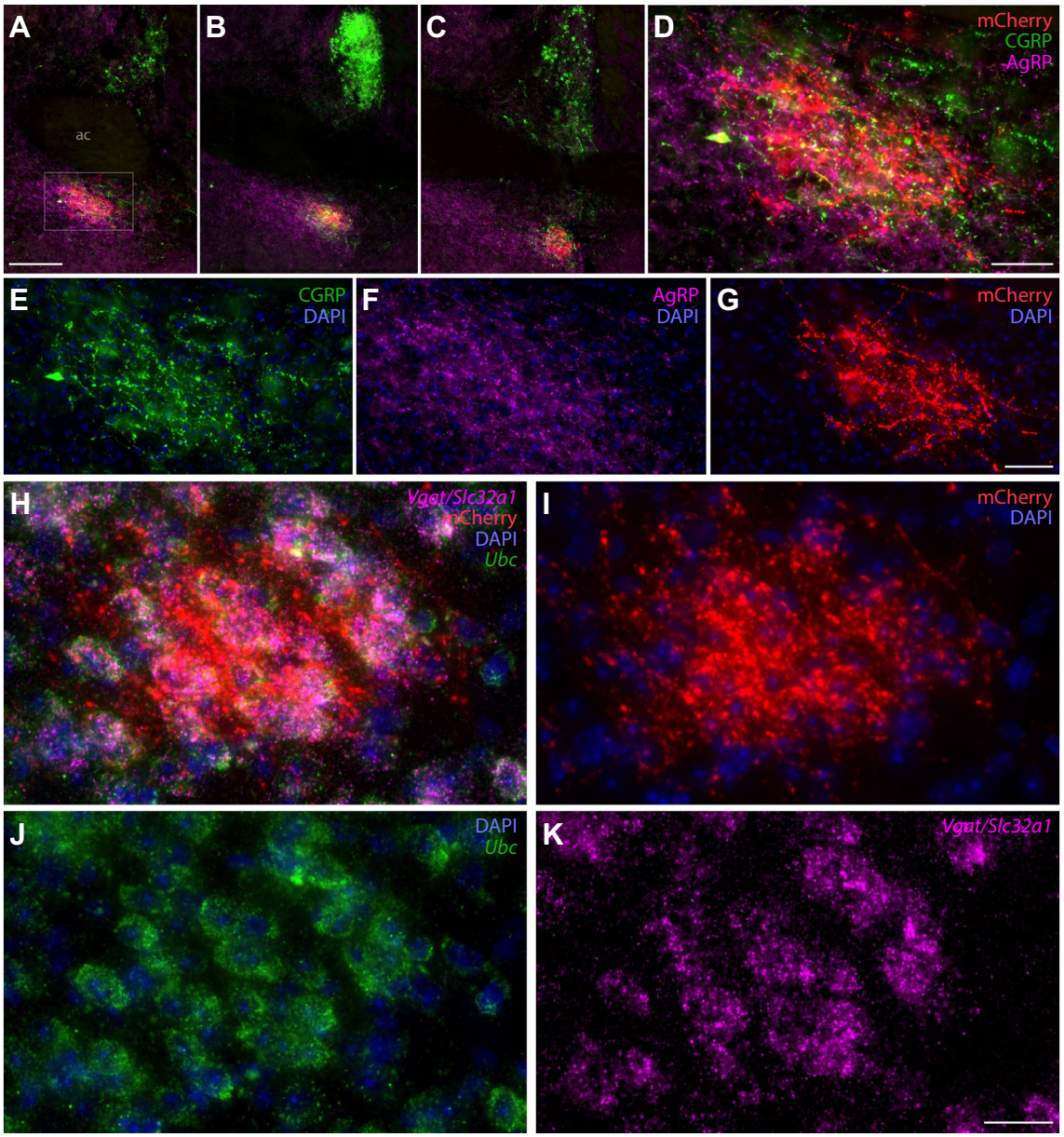

Fig. 9 **a**–**c** HSD2 axons (red, mCherry) projecting to the ventrolateral bed nucleus of the stria terminalis (BSTvL), beneath the anterior commissure form a dense terminal field ventral to the anterior commissure (ac) in rostrocaudal levels at and just rostral to its midline crossing. **d**–**g** These axons at higher magnification to highlight their closely intertwined association with separate axons immunoreactive for calcitonin gene-related peptide (CGRP, green) or agouti gene-related peptide (AgRP, magenta). **h**–**k** The HSD2 axon-terminal field in BSTvL and mRNA for the vesicular GABA transporter (Vgat/*Slc32a1*, magenta), and for the ubiquitously expressed *Ubc* (green) and DAPI nuclear counterstains, showing that HSD2 projections to BSTvL exclusively surround a population of putatively GABAergic neurons. Scale bars are 200 µm (**a**), 50 µm (**d, g**), and 20 µm (**k**) panels and apply to adjoining panels of similar size

trigeminal nucleus to form dense terminal fields flanking and streaming through the locus coeruleus (LC). The thicket of axons and boutons surrounding the LC intermingle with a neuron population containing nuclear immunoreactivity for FoxP2 (Fig. 8d–f). This FoxP2+ subpopulation is homologous to the population we named pre-LC in rats, where these neurons lie rostral to the LC. In mice, we abbreviate this population "pLC"; it includes FoxP2+ neurons receiving dense HSD2 axon terminals, flanking and streaking through the LC laterally into what is conventionally or otherwise defined as part of the medial PB, and runs medially between the LC and Barrington's nucleus (Verstegen et al. 2017). We found only sparse axonal labeling inside Barrington's nucleus, which is FoxP2-negative. The HSD2 axon-terminal distribution in the PB complex is strikingly similar to dense aggregations of AgRP-immunoreactive axons and boutons

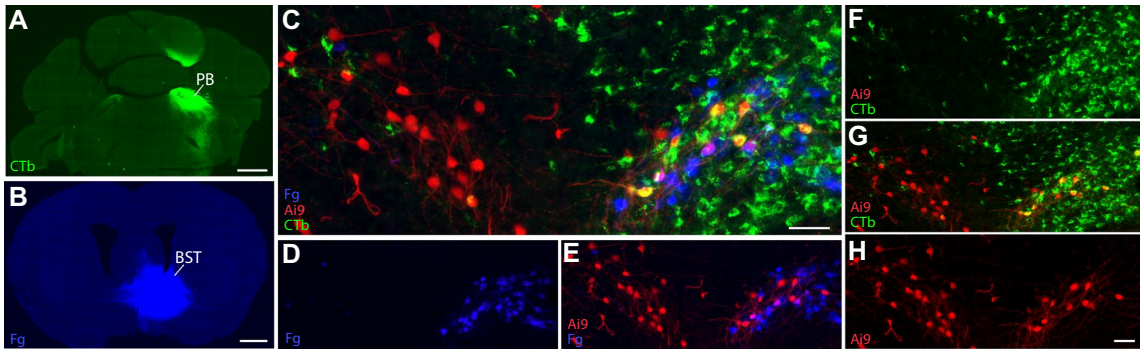

Fig. 10 Dual retrograde tracer injections reveal that most ipsilateral HSD2 neurons project to either PB or BST, not both. Large injections of cholera toxin B subunit (CTb, green) into the PB (**a**) and of Fluorogold (Fg, blue) into the BST (**b**) retrogradely labeled many HSD2 neurons in the NTS. **c**–**h** This example relies on a Cre-reporter to identify HSD2 neurons (*Hsd11b2-Cre;Ai9-lsl-tdTomato*), but immunolabeling HSD2 after dual retrograde tracer injections produced similar results in C57BL6/J mice (Table 4). Scale bars are 200 µm (**a**), 50 µm (**d, g**), and 20 µm (**k**) and apply to adjoining panels of similar size

here (Fig. 8i–m). Throughout the PB region, the distribution of AgRP axons is highly similar to that of HSD2 axon terminals, but rostral to the PB, AgRP axons form a dense terminal field in the ventrolateral periaqueductal gray matter (PAGvL), where HSD2 axonal labeling is sparse.

Beyond one or few axons branching dorsally and medially from the PB to terminate sparsely in PAGvL, most labeled axons continue rostrally and ventrally, traversing the midbrain reticular formation, ventral tegmental area, and medial forebrain bundle. In the midbrain, they track along with the medial lemniscus until it turns dorsally into the thalamus. Along the way, they form a small number of branches and boutons in the ventral midbrain without a discrete terminal field. Upon reaching the caudal hypothalamus, they produce a modest collection of branches and boutons in the parasubthalamic nucleus (PSTN, Fig. 7p). This light terminal field continues rostrally and medially through the lateral hypothalamic area (LHA), and along the way it forms modestly dense boutons and branches at mid-hypothalamic levels, in the suprafornical lateral hypothalamic area (sfLHA, Fig. 7q). Some cases contained one or two axon branches with one or few sparse boutons in the paraventricular nucleus of the hypothalamus (PVH; Fig. 7s).

Most labeled axons in the forebrain project all the way through the medial forebrain bundle and preoptic area to reach the level of the anterior commissure, where they arborize and terminate densely in a small subregion inside the ventrolateral bed nucleus of the stria terminalis (BSTvL, Fig. 7u–x). The position and appearance of this subregion is similar to that of the fusiform subnucleus in rats (Dong et al. 2001; Geerling and Loewy 2006b). This remarkably compact terminal is centered beneath and extends slightly rostral to the decussation of the anterior commissure (Fig. 9a–c), and its dense thicket of boutons envelops a tiny population of neurons that are exclusively GABAergic (Vgat/*Slc32a1*-expressing; Fig. 9h–k). Here, as in the PB, HSD2 axons intermingle with axons immunoreactive for AgRP, though these AgRP axons extends further medially, into the ventromedial BST and parastrial nucleus, which do not contain HSD2 axons. Inside the AgRP terminal field, HSD2 axon terminals also intermingle closely with a cluster of axon terminals immunoreactive for CGRP (Fig. 9d–g). CGRP axon-terminal morphology here (ventral to the anterior commissure) is distinctly different from the pericellular rosettes formed by CGRP-ir axon terminals in the oval BST (dorsal to the commissure in Fig. 9a–c). Caudal to BSTvL, one or a few axons branch laterally and course through the sublenticular substantia innominata (ansa peduncularis) and terminate sparsely in the medial subdivision of the central nucleus of the amygdala (mCeA, Fig. 7q–s).

Largely separate subpopulations of HSD2 neurons project to BSTvL or PB

Having confirmed that HSD2 neurons project axons into two primary target regions (pLC/PB and BSTvL), we next ask whether subsets of these project separately to each or if HSD2 neurons project a unitary population of axons that collateralize to reach both targets. To answer this question, we performed dual retrograde tracing. We made large injections of Fluorogold into the BST and large injections of CTb into the PB region, then compared immunolabeling for both retrograde tracers in the NTS along with HSD2 immunoreactivity ($n=2$) or red fluorescence in *Hsd11b2-Cre;Ai9-tdtomato* reporter mice ($n=2$) (Fig. 10). Each tracer labeled between 33 and 55% of ipsilateral HSD2 neurons and in every case, a large majority (72–98%) of ipsilateral HSD2 neurons contained either Fluorogold or CTb (Table 4). In three cases, we found two HSD2 neurons containing both tracers, evidence that the axon of those neurons projects

Table 4 Number and percentage of ipsilateral HSD2 neurons labeled with the retrograde tracers Fluorogold (Fg, injected into the bed nucleus of the stria terminalis) or cholera toxin B subunit (CTb, injected into the parabrachial region)

Mouse	Genotype	HSD2 neurons	HSD2 neurons with Fg (%)	HSD2 neurons with CTb (%)	HSD2 neurons labeled by Fg or CTb	HSD2 neurons labeled by both Fg and CTb (%)
714	C57BL6/J	69[a]	32 (46%)	23 (33%)	80%	2 (2.9%)
715	C57BL6/J	61[a]	20 (32%)	24 (39%)	72%	2 (3.3%)
JR1	Ai9-*Hsd11b2*^{Cre}	49[b]	21 (43%)	27 (55%)	98%	2 (4.1%)
JR3	Ai9-*Hsd11b2*^{Cre}	51[b]	23 (45%)	14 (28%)	73%	0 (0.0%)
Mean ± SEM		58 ± 5	24 ± 3 (42 ± 4%)	22 ± 2 (39 ± 7%)	81 ± 7%	1.5 ± 0.5 (2.6 ± 1%)

[a]1-in-3 series of 40 µm sections; immunolabeled for HSD2 protein

[b]1-in-4 series of 30 µm sections; red fluorescent Cre-reporter (tdTomato) for *Hsd11b2*

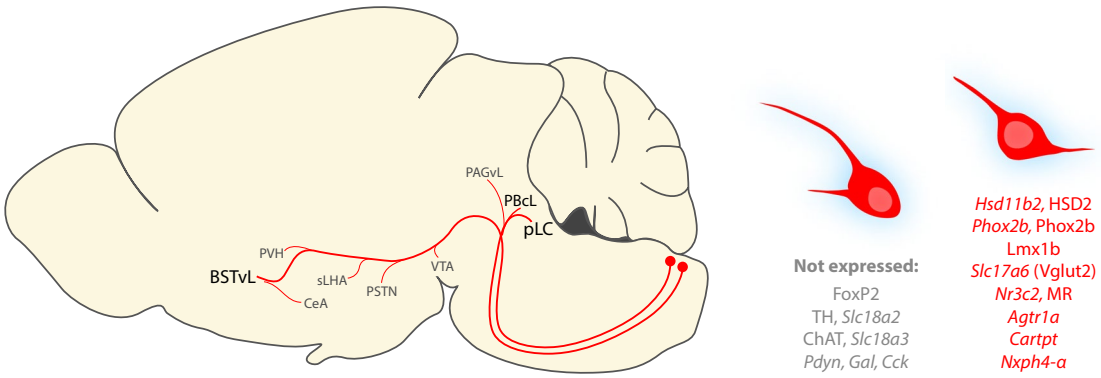

Fig. 11 Sagittal diagram summarizing the axonal projections of HSD2 neurons and genes and proteins that identify or distinguish them from surrounding NTS neurons

collaterals to both targets. In one we could not find any HSD2 neurons with both tracers. Averaged across all cases, 94% of retrogradely labeled HSD2 neurons were labeled from either BSTvL exclusively or pLC/PB exclusively. Even allowing for potential inefficiencies of dual retrograde labeling, these results suggest that a large majority of HSD2 neurons project to either pLC/PB or BSTvL, not both.

Discussion

This study extends existing genetic and neuroanatomic information on HSD2 neurons. These neurons are distinguished by their ability to sense circulating aldosterone (Geerling et al. 2006a; Resch et al. 2017), an activity pattern that is closely associated with sodium appetite (Geerling et al. 2006a; Geerling and Loewy 2007b), and the ability to promote salt intake (Formenti et al. 2013; Koneru et al. 2014; Evans et al. 2016; Jarvie and Palmiter 2017; Resch et al. 2017). By expanding on basic features first identified in rats and mice, we lay a foundation of molecular-genetic information for future work on these cells and their neural circuit connections (Fig. 11). We also identify widespread cells in all brain regions with a developmental history of *Hsd11b2* expression, we provide markers that distinguish HSD2 neurons from other NTS populations, and we identify likely target neurons and other axons converging with their axon terminals in distant brain regions. We discuss evidence that the NTS is only an adult brain region with aldosterone-sensitive neurons and why its unusual vascular permeability may allow HSD2 neurons to detect substances that do not cross the blood–brain barrier. Finally, we discuss functional implications of axonal projections from HSD2 neurons to brain regions implicated in appetite and mood.

HSD2 and aldosterone-sensitivity in the adult brain

In rats, we and others found HSD2 protein and *Hsd11b2* mRNA in three consistent locations: the NTS, the subcommissural organ (SCO), the ventrolateral subdivision of the ventromedial nucleus of the hypothalamus (VMHvL) (Roland et al. 1995; Robson et al. 1998; Geerling et al. 2006b; Askew et al. 2015). Yet in mice, radioactive in situ hybridization identified *Hsd11b2* mRNA in the NTS exclusively (Holmes et al. 2006). Here we confirm this observation, and add that *Hsd11b2* mRNA and HSD2 protein

immunoreactivity co-localize in the same NTS neurons. HSD2 neurons in the NTS, and only these neurons, express *Hsd11b2* mRNA or exhibit immunoreactivity for HSD2 in every case we have examined (now more than 100, male and female, across several strains). Unlike rats, mice do not express *Hsd11b2* mRNA or have HSD2-like immunoreactivity in the SCO or VMHvL—or any other adult brain region, under any condition we have studied. Explanations for previous reports in rats of *Hsd11b2*-like in situ hybridization or HSD2 immunoreactivity in other brain regions (outside NTS, SCO, and VMHvL) include potentially misinterpreting the background labeling inherent to radioactive in situ hybridization (Robson et al. 1998) or the neuronal nuclear cross-reactivity that we showed to be idiosyncratic to a particular sheep polyclonal antiserum used to labeling HSD2 in rats (Geerling et al. 2006b; Haque et al. 2015).

While it is possible that other cells express *Hsd11b2* at extremely low levels, or under conditions not yet tested, we used highly sensitive methods (RNAscope FISH and DAB immunohistochemistry) and had no difficulty identifying transcripts or immunoreactivity in every brain, in the NTS. Thus, if there is HSD2 elsewhere in the brain, the amount is at most substantially less than that in the NTS. Such a small amount is unlikely to be functionally relevant because the function of HSD2 is debulking intracellular glucocorticoids, and even cells that strongly express it cannot not fully metabolize glucocorticoids, leaving an intracellular concentration that is adequate to activate some MR (Funder and Myles 1996; Geerling et al. 2006a). So even if HSD2 is expressed at currently undetectable levels in other brain regions, such low-level expression is unlikely to permit aldosterone responsivity of MR relative to a 1000-fold higher concentration of circulating glucocorticoids. HSD2 neurons in the NTS are the only cells in the adult brain that robustly express both MR and HSD2 and the only cells in the adult brain with evidence for physiologic levels of circulating aldosterone producing molecular and electrophysiologic changes (Geerling et al. 2006a; Resch et al. 2017).

Having established homologous populations of HSD2 neurons in the NTS between two distantly related rodents (rats and mice), it is now of great interest whether other mammals—humans, in particular—have aldosterone-sensitive HSD2 neurons. Aldosterone-sensitive neurons and output circuits could be clinically relevant for dietary sodium intake and for better understanding and treating neuropsychiatric symptoms linked to sodium deprivation and primary hyperaldosteronism (McCance 1936; Grippo et al. 2006; Morris et al. 2006; Hlavacova and Jezova 2008; Sonino et al. 2011). We hope to identify and study these neurons in primates and in other land-dwelling mammals that require dietary sodium for survival, particularly herbivores like sheep with famously strong sodium appetites (Denton and Sabine 1961).

The HSD2 neurons overlap a leaky blood–brain barrier

In our initial description, we noted that HSD2 neurons in rats occupy a subregion of the NTS known to have an incomplete BBB (Geerling et al. 2006b). This claim stemmed from an electron microscopy report that fenestrated capillaries in the area postrema transition to a more normal BBB architecture elsewhere, and another report showing that large proteins including immunoglobulins leak from blood vessels in the subpostremal NTS (Gross et al. 1990; Broadwell and Sofroniew 1993). Here we show that the cell bodies and dendrites of many HSD2 neurons lie within this transition zone, surrounded by extracellular leakage of Fluorogold and immunoglobulins from the vasculature. The neuropil here is not as leaky as the area postrema, but is distinctly different from the rest of the brainstem. This new, direct evidence in mice supports our hypothesis that HSD2 neurons and surrounding NTS neurons may have unusually high exposure to circulating proteins and other substances like aldosterone, which is excluded from or actively transported out of the brain (Pardridge and Mietus 1979; Ueda et al. 1992; Funder and Myles 1996; Uhr et al. 2002; Geerling and Loewy 2009). We propose that this enhanced exposure to blood-borne substances allows HSD2 neurons to monitor aldosterone and other humoral signals to an extent that would be impossible elsewhere in the brain. A corollary of this prediction is that HSD2 neurons may be uniquely accessible to drugs that poorly cross the BBB, which may be therapeutically relevant. If humans have HSD2 neurons, immunolabeling brainstem tissue for immunoglobulins (Broadwell and Sofroniew 1993) may clarify whether human HSD2 neurons lie in a region with similarly enhanced BBB permeability.

Previous studies of central angiotensin II effects often focused on circumventricular organs in the lamina terminalis (Simpson and Routtenberg 1978; McKinley et al. 1992), and some authors ignore the large extent of NTS tissue that is permeable to blood-borne substances. The penetration of larger proteins into the region surrounding HSD2 neurons suggests that they also have access to smaller peptide hormones like angiotensin II. This new information, along with now three complementary types of evidence that HSD2 neurons express the type 1a angiotensin II receptor (*Agtr1a*-GFP and *Agtr1a* mRNA expression here, confirming the original discovery with RNA-Seq) gives context to evidence that HSD2 neurons exhibit losartan-blockable spiking activity when angiotensin II is applied to ex vivo brainstem slices (Resch et al. 2017).

As the only aldosterone-sensitive cells in the adult brain, and as one of a limited number of neuron subtypes capable of responding to angiotensin II, HSD2 neurons may be the only cells in the brain that directly sense and integrate both endocrine signals of sodium and volume deficiency.

Our findings further support the possibility that HSD2 neurons mediate part of a "synergy" between aldosterone and angiotensin II (Resch et al. 2017) where, at least in rats, subthreshold doses of these hormones together produce more salt intake than would be predicted by adding their individual effects (Epstein 1982; Fluharty and Epstein 1983). Aldosterone and angiotensin II acting on HSD2 neurons may augment, but does not preclude a convergent role for angiotensin II-activated neurons in the lamina terminalis that project axons to BSTvL (Sunn et al. 2003; Matsuda et al. 2017).

Potentially more important than these two endocrine signals is the still unclear role of synaptic input to HSD2 neurons. HSD2 neurons are coated in GABAergic and glutamatergic appositions from presynaptic boutons (Shin et al. 2009), which originate from local interneurons (Sequeira et al. 2006), the vagus nerve (Shin et al. 2009), and forebrain nuclei (Geerling and Loewy 2006a; Geerling et al. 2010). However, functional evidence for vagal synaptic input has been elusive, and HSD2 neurons have the uncommon property of firing pacemaker-type action potentials in ex vivo slices after dietary sodium deprivation or systemic aldosterone treatment (Resch et al. 2017). It is unclear whether intrinsic, synaptic, or humoral signals primarily sculpt the activity of HSD2 neurons in vivo, and resolving this uncertainty is important for understanding the neurophysiology of sodium appetite.

Gene and protein markers for HSD2 neurons

Full and accurate information on cellular gene and protein markers can expand our options for identifying and targeting experimental tools and therapies to functionally specific cells of interest in mice and other species. Without expansively discussing all the gene and protein markers above, here we highlight some new, useful, or functionally relevant details.

We showed in rats that HSD2 neurons are a subset of Phox2b+ glutamatergic neurons (Geerling et al. 2008), yet distinct from other NTS subpopulations (Geerling et al. 2006b), and here we confirm their Phox2b-derived developmental identity in mice, finding ubiquitous co-localization between HSD2 and both *Phox2b* mRNA and nuclear Phox2b immunoreactivity. Unexpectedly, we also found the nuclear transcription factor Lmx1b in some HSD2 neurons. Lmx1b, which is expressed in a subset of NTS neurons (Dai et al. 2008), splits the HSD2 neurons into two previously unrecognized subpopulations, with roughly one-third (dorsal and lateral) expressing it, and two-thirds (ventral and medial) lacking Lmx1b. It will be important to learn whether and how the presence or absence of Lmx1b influences gene expression, biases axonal projections, or influences the function of HSD2 neurons.

Beyond validating the RNA-seq discovery that HSD2 neurons uniformly express the glutamatergic marker *Slc17a6* and the mineralocorticoid receptor *Nr2c3*, we confirm that HSD2 neurons are entirely distinct from NTS catecholamine neurons based on their lack of both TH immunoreactivity and mRNA for the vesicular monoamine transporter VMAT2 (*Slc18a2*). We also confirm that they are non-cholinergic based on the lack of ChAT immunoreactivity and mRNA for the vesicular acetylcholine transporter (*Slc18a3*). We find that HSD2 neurons are mutually exclusive with most other populations of neuropeptidergic neurons in the NTS including prodynorphin, cholecystokinin, and galanin, but then identify cocaine and amphetamine-regulated transcript in roughly half, and an obscure neuropeptide gene, *Nxph4*, in virtually all HSD2 neurons. Both these transcripts are found in other NTS neurons, and neither is specific to HSD2 neurons. Besides *Hsd11b2*, we have not identified any genetic markers that uniquely identify HSD2 neurons.

Functional implications of HSD2 axonal projections

Using conventional protein tracers to construct a map of HSD2 axonal projections in rats (Geerling and Loewy 2006b) required precise injections of an anterograde tracer into the HSD2 subregion to label all axons emerging from this region of the NTS, then injecting a retrograde tracer (CTb) into each target region and double-immunolabeling HSD2 and CTb in many cases to determine which brain regions receive axonal input from HSD2 neurons. This labor-intensive approach predated Cre-conditional tracing tools and Cre-driver mice for *Hsd11b2* and, despite retrograde tracer injections covering all NTS target regions, left open the possibility of false-positive results when CTb enters axons passing through the injection site without synapsing there (Chen and Aston-Jones 1995). Nonetheless, our HSD2 projection map here in mice (Fig. 11) largely confirms our conclusions from conventional tracing in rats (Geerling and Loewy 2006b). The power of Cre-conditional genetic tracing allows us now to draw more definitive conclusions about which brain regions do or do not receive axonal projections from HSD2 neurons, and here we discuss functional implications of this now-comprehensive projection map that extends recent data in mice (Jarvie and Palmiter 2017; Resch et al. 2017).

First, it is clear now that *little or no HSD2 axonal output targets neurons inside the NTS*. The dense labeling of dendrites and proximal axons prevents us from fully excluding the possibility that some HSD2 axons form boutons while exiting the NTS, but we see no evidence that they emit intranuclear collaterals. They do not produce any projections, varicosities or boutons targeting rostral NTS subnuclei that relay gustatory information. This distinction was left ambiguous in our original tracing study because anterograde tracer

injections invariably spread to local interneurons, which project densely inside the NTS, and because we found a few HSD2 neurons retrogradely labeled after injecting CTb immediately rostral to the HSD2 neurons (Geerling and Loewy 2006b). Cre-conditional tracing eliminates these confounds because only neurons that express *Hsd11b2* at or after the time of AAV injection can produce the genetically encoded tracer, so labeled axons emit exclusively from HSD2 neurons. That HSD2 neurons provide minimal (or no) projections within the NTS that places them in a previously described class of NTS neurons that lack local, axon-collateral projections (Kawai and Senba 1996; Kawai 2018), with important functional implications for HSD2 neurons and, by extension, aldosterone. That is, whether or not HSD2 neurons influence sodium taste detection or any autonomic reflexes, it is highly unlikely that they exert such influence directly within the brain's first-order gustatory and viscerosensory nucleus, the NTS.

Second, *HSD2 neurons do not project axons to autonomic regions of the ventrolateral medulla*. The ventrolateral medulla funnels most of the brain's pre-autonomic output through discrete populations of respiratory, sympathetic, and parasympathetic (vagal) premotor neurons. Many NTS neurons project to one or more of these pre-autonomic populations, yet HSD2 neurons project past this region without issuing a single axon branch or bouton. The total absence of HSD2 axonal projections to the ventrolateral medulla is unlikely to be an artifact of AAV tropism or to reflect inability of NTS axons to transport our fluorescently proteins tracers because in our ongoing work with glutamatergic and catecholaminergic Cre-driver mice, injecting the same AAVs into the same NTS coordinates abundantly labels axonal projections to the ventrolateral medulla (SG and JG, unpublished observations). Further, injecting CTb into the ventrolateral medulla in rats, despite labeling many NTS neurons, does not label a single HSD2 neuron (Geerling and Loewy 2006b). NTS neurons are best-known for textbook autonomic reflexes like the baroreflex, in which they receive direct synaptic input from viscerosensory nerves then relay this information to pre-autonomic neurons in the ventrolateral medulla and to preganglionic parasympathetic neurons in the dorsal motor nucleus of the vagus or nucleus ambiguus. It is remarkable that an entire subpopulation of NTS projection neurons fails to send even a single axon collateral into this important brainstem region, and our negative data in this regard highlight the power of cell type-specific axon labeling. We cannot exclude the possibility that HSD2 neurons form en passant synapses on interneurons in the reticular formation (or on dorsal dendrites of dorsal vagal motor neurons), but our findings indicate that they do not exert a direct effect on autonomic motor or premotor neurons in the ventrolateral medulla. This is important because we and others initially predicted that HSD2 neurons, or other aldosterone-sensitive neurons, increase blood pressure (Gomez-Sanchez 1986; Guyenet 2006; Geerling and Loewy 2009). Instead, our neuroanatomical data strongly suggest that HSD2 neurons influence behavior, not autonomic function. Entirely excluding an autonomic role would be difficult, but we have shown that stimulating HSD2 neurons alters ingestive behavior without changing blood pressure or heart rate (Resch et al. 2017). Even if the functional role of HSD2 neurons—and by extension, aldosterone—were to include an autonomic effect, that effect would at minimum violate the wiring efficiency principle of Cajal by requiring an inefficient, long-loop path through the forebrain (PVH, LHA, BST and/or CeA) and back to autonomic effector neurons in the hindbrain or spinal cord.

Third, *HSD2 projections to sites outside two major terminal fields are sparse*. The number and density of boutons targeting the PB and BSTvL are qualitatively greater than the rest of their other projections combined, but before addressing these two primary target regions, we briefly address their minor terminal sites relative to the output targets we initially proposed in rats (Geerling and Loewy 2006b). Outside pLC/PB, HSD2 axons do not arborize or terminate significantly in the brainstem except for a vanishingly sparse projection to PAGvL and sparse branches and boutons in the vicinity of the ventral tegmental area in the ventral midbrain. We identified a similarly sparse axonal projection to the VTA in rats, and CTb injections there retrogradely labeled a modest number of HSD2 neurons. Learning whether these boutons synapse on dopamine neurons, or the GABAergic interneurons that inhibit them, or some other neurons will require additional work, and sagittal sections would be advantageous for identifying more boutons per slice in this sparse rostrocaudal terminal field. Rostral to the midbrain, slightly more varicosities target caudal levels of the lateral-most LHA (PSTN) up through the mid-rostral LHA above the fornix (sLHA). Rostral to these sites, the mCeA and PVH receive vanishingly sparse HSD2 axons and boutons, with no more than one or a few labeled boutons across 1–3 sections per brain, complementing our finding in rats that only small numbers of HSD2 neurons were retrogradely labeled in cases with CTb injected into these sites (see Fig. 3, panels B-D in Geerling and Loewy 2006b). The functional relevance of sparse, direct HSD2 projections to the hypothalamus and amygdala is unclear, and may be less important than heavy, relayed projections of FoxP2+ target neurons in pLC/PB to the LHA, PVH, and other forebrain sites (Shin et al. 2011). One likely exception is the mCeA, which despite our prediction that it receives PB-relayed input from HSD2 neurons (HSD2◊PB◊mCeA) (Geerling and Loewy 2006a) receives no axonal projections from the FoxP2+ subtype of PB neurons that appear to be targeted by HSD2 neurons (Shin et al. 2011).

Fourth, *HSD2 axons form dense terminal fields surrounding FoxP2+ neurons in pLC and PBcL, converging with AgRP projections from the hypothalamus*. We named and defined the pre-locus coeruleus in rats as a discrete population of neurons that receive heavy input from the HSD2 subregion of the NTS (Geerling and Loewy 2006b), produce c-Fos in response to sodium deprivation (Geerling and Loewy 2007c), and express FoxP2 (Geerling et al. 2011). We also showed that this population is the major target of projections from the PVH to the upper brainstem (Geerling et al. 2010). Here, we add AgRP axonal projections to the list of its major inputs. AgRP terminal fields in PB are strikingly similar to the HSD2 terminal pattern. Sparser HSD2 and AgRP fibers and boutons extend into adjacent PB regions including the dorsal and external lateral PB subnuclei (Essner et al. 2017), but their density is greatest in pLC and the same, thin subregion of PBcL. Such strikingly similar terminal patterns of projections from distant brain regions suggests that during development the same molecular signal(s) attract and stabilize synapses from these two neuron types onto a specific subset of FoxP2+ PB neurons.

Convergent input from HSD2, AgRP, and PVH neurons onto FoxP2+ neurons in pLC and PBcL may be highly significant for appetite control. AgRP neuron activity promotes hunger (Aponte et al. 2011; Krashes et al. 2011), and eliminating them causes anorexia (Luquet et al. 2005). They release the inhibitory neurotransmitter GABA (Tong et al. 2008; Wu et al. 2009) and AgRP, an inverse agonist that reduces melanocortin receptor activity (Ollmann et al. 1997; Haskell-Luevano and Monck 2001; Nijenhuis et al. 2001). AgRP neurons promote hunger via projections to several brain regions (Betley et al. 2013), but their inhibitory projections to the PB region specifically have been shown to prevent anorexia (Wu et al. 2009). In contrast to inhibitory, hunger-promoting AgRP neurons, PVH neurons are excitatory and reduce appetite via synaptic glutamate release in the PB (Garfield et al. 2015). HSD2 neurons also release glutamate and inhibit appetite, unless the food on offer is salty (Resch et al. 2017). There are many nuances to appetite control, but our neuroanatomical data suggest that a highly specific pair of FoxP2+ neuron subpopulations—pLC and PBcL—receive convergent inputs from HSD2, AgRP, and PVH neurons. We predict that one or both of these FoxP2+ populations integrates hunger-reducing excitatory (HSD2 and PVH) and hunger-promoting inhibitory (AgRP/GABA) inputs and relays the balance of these signals as an excitatory (presumably anorexic) signal to forebrain circuits that control ingestive behavior.

We mapped the axonal projections of FoxP2+ pLC/PBcL neurons to the forebrain using conventional anterograde and retrograde tracing techniques in rats, and found that these relay neurons project heavily to diencephalic regions including the PVH, LHA, and paraventricular thalamic nucleus (Shin et al. 2011). Beyond just appetite, these sites are thought to be core nodes in the neural circuits responsible for stressful and dysphoric mood states (Bard 1928; Sawchenko et al. 1996; Price and Drevets 2012). HSD2 neurons project sparsely to some of these sites, but their primary influence (and by extension, aldosterone's primary influence) on this forebrain network is probably mediated by the much heavier projections of FoxP2+ relay neurons in pLC and PBcL. We predict that these relay neurons represent a bottleneck node for integrating convergent excitation by PVH and HSD2 neurons (hunger-reducing, dysphoria-promoting) with inhibition by AgRP neurons (hunger-promoting, dysphoria-reducing), and other inputs that in aggregate tilt the balance of activity in this forebrain network toward a state of dysphoria and anorexia (PVH and/or HSD2 active; AgRP quiet) or hunger (PVH and HSD2 quiet; AgRP active). This testable model, with FoxP2+ pLC/PBcL neurons as a nodal choke point, may provide mechanistic insights to what are at present phenomenological links between appetite and mood dysregulation and disease states with excess aldosterone, such as heart failure (Lesman-Leegte et al. 2006; Rutledge et al. 2006).

The disease state with most obvious relevance to the present work is hyperaldosteronism. Whether it is "secondary" (production in response to a sodium or volume deficit, or to an excess of potassium) or "primary" (overproduction by an adrenal tumor, known as Conn's syndrome), hyperaldosteronism causes mood dysphoria and anhedonia (Malinow and Lion 1979; Grippo et al. 2006; Morris et al. 2006; Sonino et al. 2006, 2011; Hlavacova and Jezova 2008; Hlavacova et al. 2012; Velema et al. 2017; Reincke 2018). All psychiatric symptoms result from changing neural circuit activity, but the specific mechanisms linking hyperaldosteronism to mood circuits in the brain remain unknown. Prior work on corticosteroids and mood focused largely on glucocorticoids acting on MR in the hippocampus and other limbic regions lacking HSD2 (de Kloet et al. 2016). For hyperaldosteronism, our work predicts a simple, testable model where aldosterone boosts the activity of HSD2 neurons, their axons excite FoxP2+ relay neurons in pLC/PBcL, and their projections to the diencephalon activate a stress-associated network of forebrain regions that produce anorexia, anhedonia, and other dysphoric symptoms. If so, blunting HSD2 neuron activity with a mineralocorticoid antagonist or salt consumption (with or without other interventions such as food restriction to increase AgRP inhibition of pLC/PBcL neurons) might dampen activity in this forebrain network and ameliorate psychiatric sequelae of hyperaldosteronism. While it is unclear whether this aldosterone-driven circuit plays a role in mood disorders generally (without hyperaldosteronism), mood associations of mineralocorticoid levels and gene variants in human MR are fueling renewed interest in testing MR receptor-binding compounds in clinically depressed patients (Murck et al. 2014). Clearly, the existence

of MR-expressing, aldosterone-sensitive neurons and their relayed projections to an aversive forebrain network offers a testable circuit basis for refining such efforts. This accessible, tangible, viscerosensory pathway holds the potential for new insights into the ethological and neural circuit basis of mood disorders.

Separate from these functional implications, mice and rats diverge in important ways in their geometry of HSD2 axonal projections to, and FoxP2+ neuron distributions within, the PB region, and this divergence highlights an important and pervasive challenge in translational neuroscience. In mice, the cluster of lateral PB, FoxP2+ neurons receiving HSD2 (and AgRP) axons clearly lies within PBcL (dorsomedial to PBeL, which is FoxP2-negative in Fig. 8), yet in rats these NTS terminals and their FoxP2+ target neurons cascade along and through the ventrolateral edge of the superior cerebellar peduncle, which by previous conventional belongs to the inner subdivision of PBeL (Herbert and Saper 1990; Geerling and Loewy 2006b). That an identical pair of inputs and target neurons would fall into entirely separate PB subnuclei in two rodent species calls into question the utility of conventional, landmark-based, cytoarchitectural definitions for neuron populations. Even worse, our "pre"-LC cluster of FoxP2+ neurons (and their HSD2 afferents) are not at all rostral to the LC in mice, and instead wrap haphazardly around and through the LC. This unfortunate species difference in the spatial relationship between the pre-LC and LC undercuts the anatomic basis for its name in rats when applied to mice. Further complicating things, HSD2 axon terminals in mice extend lateral through the LC and into the caudal medial PB subnucleus, which in rats contains neurons activated by salt taste (Geerling and Loewy 2007c). Without yet knowing the gustatory Fos distribution in mice, this raises the possibility that HSD2 neurons in mice, but not rats, modulate gustatory sodium detection. Without gene and protein markers, it would be impossible to understand and classify homologies (or lack thereof) between target neurons and axon terminals in the PB region, even between two rodent species. As our ultimate goal is to develop a better understanding of these neural circuits in an evolutionarily distant primate (humans), these examples show why molecular markers and genetically targeted techniques, rather than cytoarchitecture, is necessary for translating neuroanatomical findings across species.

Fifth, *a separate subset of HSD2 axons densely target a tiny subregion within BSTvL*. We and others have written at length about the anatomy, connectivity, and functional relevance of this dense, focal projection of HSD2 neurons to BSTvL (Dong et al. 2001; Geerling and Loewy 2006b, 2008, 2009; Shin et al. 2008). Beyond sodium appetite, other findings implicate this region in the dysphoric state of opioid withdrawal (Aston-Jones et al. 1999) and implicate other regions of the BST in stress and anxiety (Walker et al. 2003), raising the possibility that HSD2 neurons promote dysphoric mood through their projections to BST similar to (or instead of) FoxP2+ relay neurons in the PB region.

Besides input from the aldosterone-modulated, sodium deprivation-activated HSD2 neurons, neurons in BSTvL integrate information from infralimbic and insular cortex, midline and intralaminar thalamic nuclei, central and basal amygdala, several hypothalamic nuclei, and specific brainstem neurons including serotonin neurons in the dorsal raphe (Shin et al. 2008). Among these input connections, we confirm here that BSTvL receives input from AgRP neurons in the arcuate nucleus of the hypothalamus (Shin et al. 2008) and a subset of CGRP neurons in PB (Geerling and Loewy 2006b; Resch et al. 2017). Optogenetically stimulating AgRP axons here potently increases food intake (Betley et al. 2013). The function of CGRP afferents in BSTvL is unclear, but PB CGRP neurons in general relay interoceptive aversive signals, triggering anorexia and alerting responses (Saper 2016; Palmiter 2018). BSTvL also receives heavy input from noradrenergic A1 and A2 neurons in the medulla (Terenzi and Ingram 1995; Geerling and Loewy 2006b), and norepinephrine acts pre-synaptically in BSTvL via alpha-2-adrenoreceptors to inhibit glutamate release (Egli et al. 2005; Shields et al. 2009). It is unknown whether glutamatergic HSD2 axons are among those suppressed by this presynaptic mechanism, but this convergence makes the BSTvL a strong candidate locus for the previously unexplained phenomenon of sodium appetite induced by an alpha-2-adrenoreceptor antagonist, yohimbine (Fitts 1991).

Also of note, BSTvL receives sparse input from angiotensin II-activated neurons in the subfornical organ (SFO) (Sunn et al. 2003; Shin et al. 2008; Matsuda et al. 2017), and before learning that HSD2 neurons can detect angiotensin II we had predicted that SFO delivers angiotensin II-related input to BSTvL for integration with aldosterone-related input from HSD2 neurons to promote sodium appetite (Geerling and Loewy 2006b, 2008). Independent experiments then showed that *Agtr1a*-expressing SFO neurons (Matsuda et al. 2017) and HSD2 neurons (Resch et al. 2017) each promote salt intake via BSTvL. It remains unclear whether they activate the same BSTvL target neurons and how their activity interacts with other BSTvL afferents to modulate sodium appetite, mood, or other behaviors. Destroying the BST greatly reduces sodium appetite (Zardetto-Smith et al. 1994) and neurons in the basal forebrain, in or near BSTvL, exhibit sodium appetite-related changes in spiking activity and play a role in sodium appetite-associated behaviors (Tindell et al. 2006; Chang et al. 2017). BSTvL is likely central to all these phenomena, but because its neurons project heavily into and through the adjacent basal forebrain (Dong et al. 2001), it is unclear whether the neurons described by other investigators are the same HSD2-targeted, GABAergic neurons we identify here or are the output targets of these neurons in

a neighboring region of the basal forebrain. In either case, evidence in rats that unit activity here tracks the behavioral shift from "disliking" to "liking" salt (Tindell et al. 2006), coupled with evidence that activating HSD2 axon terminals in BSTvL increases saline intake (Resch et al. 2017) highlights this region as a core component of the brain's "hedonic switch" responsible for sodium appetite.

In conclusion, our findings complement and extend previous information about HSD2 neurons, supporting the likelihood that HSD2 neurons can sense circulating hormones including angiotensin II and aldosterone. We provide a set of genetic markers as a molecular-genetic foundation for distinguishing HSD2 neurons from other NTS populations. Our detailed, map of HSD2 axonal projections should guide future work on downstream, aldosterone-sensitive brain circuits responding to body sodium deficiency. We know already that HSD2 neurons and their downstream targets promote sodium appetite, but they may also influence stress and mood circuits to produce dysphoric, anhedonic, and anorexic symptoms identified in rodents and humans with primary or secondary hyperaldosteronism.

Acknowledgements We thank Richard Palmiter and Aniko Fejes-Toth for sharing *Hsd11b2* Cre-driver mice; David Olson for L10GFP Cre-reporter mice; and Justin Grobe, Huxing Cui, and Kenji Saito for *Agtr1a*-GFP mice and brainstem tissue. Hideki Enomoto of Kobe University generously provided an aliquot of GP-anti-Phox2b, and Carmen Birchmeier generously provided an aliquot of GP-anti-Lmx1b antiserum. Finally, we thank Brad Lowell for mentorship and for material support for much of this work.

Funding Grant sponsors: NIH F32 DK103387 (JMR). NIH K08 NS099425 (JCG). Aging Mind and Brain Initiative, University of Iowa Center for Aging (JCG).

Compliance with ethical standards

Ethical approval All procedures performed in studies involving animals were in accordance with the ethical standards of the institution or practice at which the studies were conducted.

References

Aponte Y, Atasoy D, Sternson SM (2011) AGRP neurons are sufficient to orchestrate feeding behavior rapidly and without training. Nat Neurosci 14(3):351–355

Arriza JL, Simerly RB, Swanson LW, Evans RM (1988) The neuronal mineralocorticoid receptor as a mediator of glucocorticoid response. Neuron 1(9):887–900

Askew ML, Muckelrath HD, Johnston JR, Curtis KS (2015) Neuroanatomical association of hypothalamic HSD2-containing neurons with ERalpha, catecholamines, or oxytocin: implications for feeding? Front Syst Neurosci 9:91

Aston-Jones G, Delfs JM, Druhan J, Zhu Y (1999) The bed nucleus of the stria terminalis. A target site for noradrenergic actions in opiate withdrawal. Ann N Y Acad Sci 877:486–498

Bard P (1928) A diencephalic mechanism for the expression of rage with special reference to the sympathetic nervous system. Am J Physiol 84(3):490–515

Betley JN, Cao ZF, Ritola KD, Sternson SM (2013) Parallel, redundant circuit organization for homeostatic control of feeding behavior. Cell 155(6):1337–1350

Broadwell RD, Sofroniew MV (1993) Serum proteins bypass the blood-brain fluid barriers for extracellular entry to the central nervous system. Exp Neurol 120(2):245–263

Chang RB, Strochlic DE, Williams EK, Umans BD, Liberles SD (2015) Vagal sensory neuron subtypes that differentially control breathing. Cell 161(3):622–633

Chang SE, Smedley EB, Stansfield KJ, Stott JJ, Smith KS (2017) optogenetic inhibition of ventral pallidum neurons impairs context-driven salt seeking. J Neurosci 37(23):5670–5680

Chen S, Aston-Jones G (1995) Evidence that cholera toxin B subunit (CTb) can be avidly taken up and transported by fibers of passage. Brain Res 674(1):107–111

Craig AD (2002) How do you feel? Interoception: the sense of the physiological condition of the body. Nat Rev Neurosci 3(8):655–666

Dai JX, Hu ZL, Shi M, Guo C, Ding YQ (2008) Postnatal ontogeny of the transcription factor Lmx1b in the mouse central nervous system. J Comp Neurol 509(4):341–355

de Kloet ER, Otte C, Kumsta R, Kok L, Hillegers MH, Hasselmann H, Kliegel D, Joels M (2016) Stress and depression: a crucial role of the mineralocorticoid receptor. J Neuroendocrinol 28(8)

Denton DA, Sabine JR (1961) The selective appetite for Na ions shown by Na ion-deficient sheep. J Physiol 157:97–116

Diaz R, Brown RW, Seckl JR (1998) Distinct ontogeny of glucocorticoid and mineralocorticoid receptor and 11beta-hydroxysteroid dehydrogenase types I and II mRNAs in the fetal rat brain suggest a complex control of glucocorticoid actions. J Neurosci 18(7):2570–2580

Dong HW (2008) Allen reference atlas: a digital color brain atlas of the C57Black/6J male mouse. Wiley. ix, Hoboken, 366 p. p

Dong HW, Petrovich GD, Watts AG, Swanson LW (2001) Basic organization of projections from the oval and fusiform nuclei of the bed nuclei of the stria terminalis in adult rat brain. J Comp Neurol 436(4):430–455

Egli RE, Kash TL, Choo K, Savchenko V, Matthews RT, Blakely RD, Winder DG (2005) Norepinephrine modulates glutamatergic transmission in the bed nucleus of the stria terminalis. Neuropsychopharmacology 30(4):657–668

Epstein AN (1982) Mineralocorticoids and cerebral angiotensin may act together to produce sodium appetite. Peptides 3(3):493–494

Essner RA, Smith AG, Jamnik AA, Ryba AR, Trutner ZD, Carter ME (2017) AgRP neurons can increase food intake during conditions of appetite suppression and inhibit anorexigenic parabrachial neurons. J Neurosci 37(36):8678–8687

Evans LC, Ivy JR, Wyrwoll C, McNairn JA, Menzies RI, Christensen TH, Al-Dujaili EA, Kenyon CJ, Mullins JJ, Seckl JR, Holmes MC, Bailey MA (2016) Conditional deletion of Hsd11b2 in the brain causes salt appetite and hypertension. Circulation 133(14):1360–1370

Fitts DA (1991) Effects of lesions of the ventral ventral median preoptic nucleus or subfornical organ on drinking and salt appetite after deoxycorticosterone acetate or yohimbine. Behav Neurosci 105(5):721–726

Fluharty SJ, Epstein AN (1983) Sodium appetite elicited by intracerebroventricular infusion of angiotensin II in the rat: II. Synergistic interaction with systemic mineralocorticoids. Behav Neurosci 97(5):746–758

Formenti S, Bassi M, Nakamura NB, Schoorlemmer GH, Menani JV, Colombari E (2013) Hindbrain mineralocorticoid mechanisms on sodium appetite. Am J Physiol Regul Integr Comp Physiol 304(3):R252–R259

Franklin KBJ, Paxinos G (2013) Paxinos and Franklin's The mouse brain in stereotaxic coordinates. Academic Press, Amsterdam

Funder J, Myles K (1996) Exclusion of corticosterone from epithelial mineralocorticoid receptors is insufficient for selectivity of aldosterone action: in vivo binding studies. Endocrinology 137(12):5264–5268

Funder JW, Pearce PT, Smith R, Smith AI (1988) Mineralocorticoid action: target tissue specificity is enzyme, not receptor, mediated. Science 242(4878):583–585

Garfield AS, Li C, Madara JC, Shah BP, Webber E, Steger JS, Campbell JN, Gavrilova O, Lee CE, Olson DP, Elmquist JK, Tannous BA, Krashes MJ, Lowell BB (2015) A neural basis for melanocortin-4 receptor-regulated appetite. Nat Neurosci 18(6):863–871

Geerling JC, Loewy AD (2006a) Aldosterone-sensitive neurons in the nucleus of the solitary tract: bidirectional connections with the central nucleus of the amygdala. J Comp Neurol 497(4):646–657

Geerling JC, Loewy AD (2006b) Aldosterone-sensitive neurons in the nucleus of the solitary tract: efferent projections. J Comp Neurol 497(2):223–250

Geerling JC, Loewy AD (2006c) Aldosterone-sensitive NTS neurons are inhibited by saline ingestion during chronic mineralocorticoid treatment. Brain Res 1115(1):54–64

Geerling JC, Loewy AD (2007a) 11beta-hydroxysteroid dehydrogenase 2 vs. transgene: discrepant loci of expression in the adult brain. Am J Physiol Renal Physiol 293(1):F440–F441 **(author reply F442–F443)**

Geerling JC, Loewy AD (2007b) Sodium depletion activates the aldosterone-sensitive neurons in the NTS independently of thirst. Am J Physiol Regul Integr Comp Physiol 292(3):R1338–R1348

Geerling JC, Loewy AD (2007c) Sodium deprivation and salt intake activate separate neuronal subpopulations in the nucleus of the solitary tract and the parabrachial complex. J Comp Neurol 504(4):379–403

Geerling JC, Loewy AD (2008) Central regulation of sodium appetite. Exp Physiol 93(2):177–209

Geerling JC, Loewy AD (2009) Aldosterone in the brain. Am J Physiol Renal Physiol 297(3):F559–F576

Geerling JC, Engeland WC, Kawata M, Loewy AD (2006a) Aldosterone target neurons in the nucleus tractus solitarius drive sodium appetite. J Neurosci 26(2):411–417

Geerling JC, Kawata M, Loewy AD (2006b) Aldosterone-sensitive neurons in the rat central nervous system. J Comp Neurol 494(3):515–527

Geerling JC, Chimenti PC, Loewy AD (2008) Phox2b expression in the aldosterone-sensitive HSD2 neurons of the NTS. Brain Res 1226:82–88

Geerling JC, Shin JW, Chimenti PC, Loewy AD (2010) Paraventricular hypothalamic nucleus: axonal projections to the brainstem. J Comp Neurol 518(9):1460–1499

Geerling JC, Stein MK, Miller RL, Shin JW, Gray PA, Loewy AD (2011) FoxP2 expression defines dorsolateral pontine neurons activated by sodium deprivation. Brain Res 1375:19–27

Gomez-Sanchez EP (1986) Intracerebroventricular infusion of aldosterone induces hypertension in rats. Endocrinology 118(2):819–823

Gong S, Zheng C, Doughty ML, Losos K, Didkovsky N, Schambra UB, Nowak NJ, Joyner A, Leblanc G, Hatten ME, Heintz N (2003) A gene expression atlas of the central nervous system based on bacterial artificial chromosomes. Nature 425(6961):917–925

Gonzalez AD, Wang G, Waters EM, Gonzales KL, Speth RC, Van Kempen TA, Marques-Lopes J, Young CN, Butler SD, Davisson RL, Iadecola C, Pickel VM, Pierce JP, Milner TA (2012) Distribution of angiotensin type 1a receptor-containing cells in the brains of bacterial artificial chromosome transgenic mice. Neuroscience 226:489–509

Grippo AJ, Moffitt JA, Beltz TG, Johnson AK (2006) Reduced hedonic behavior and altered cardiovascular function induced by mild sodium depletion in rats. Behav Neurosci 120(5):1133–1143

Gross PM, Wall KM, Pang JJ, Shaver SW, Wainman DS (1990) Microvascular specializations promoting rapid interstitial solute dispersion in nucleus tractus solitarius. Am J Physiol 259(6 Pt 2):R1131–R1138

Guyenet PG (2006) The sympathetic control of blood pressure. Nat Rev Neurosci 7(5):335–346

Haque M, Wilson R, Sharma K, Mills NJ, Teruyama R (2015) Localisation of 11beta-hydroxysteroid dehydrogenase type 2 in mineralocorticoid receptor expressing magnocellular neurosecretory neurones of the rat supraoptic and paraventricular nuclei. J Neuroendocrinol 27(11):835–849

Haskell-Luevano C, Monck EK (2001) Agouti-related protein functions as an inverse agonist at a constitutively active brain melanocortin-4 receptor. Regul Pept 99(1):1–7

Herbert H, Saper CB (1990) Cholecystokinin-, galanin-, and corticotropin-releasing factor-like immunoreactive projections from the nucleus of the solitary tract to the parabrachial nucleus in the rat. J Comp Neurol 293(4):581–598

Hlavacova N, Jezova D (2008) Chronic treatment with the mineralocorticoid hormone aldosterone results in increased anxiety-like behavior. Horm Behav 54(1):90–97

Hlavacova N, Wes PD, Ondrejcakova M, Flynn ME, Poundstone PK, Babic S, Murck H, Jezova D (2012) Subchronic treatment with aldosterone induces depression-like behaviours and gene expression changes relevant to major depressive disorder. Int J Neuropsychopharmacol 15(2):247–265

Holmes MC, Sangra M, French KL, Whittle IR, Paterson J, Mullins JJ, Seckl JR (2006) 11beta-Hydroxysteroid dehydrogenase type 2 protects the neonatal cerebellum from deleterious effects of glucocorticoids. Neuroscience 137(3):865–873

Jarvie BC, Palmiter RD (2017) HSD2 neurons in the hindbrain drive sodium appetite. Nat Neurosci 20(2):167–169

Jellinck PH, Monder C, McEwen BS, Sakai RR (1993) Differential inhibition of 11 beta-hydroxysteroid dehydrogenase by carbenoxolone in rat brain regions and peripheral tissues. J Steroid Biochem Mol Biol 46(2):209–213

Kang BJ, Chang DA, Mackay DD, West GH, Moreira TS, Takakura AC, Gwilt JM, Guyenet PG, Stornetta RL (2007) Central nervous system distribution of the transcription factor Phox2b in the adult rat. J Comp Neurol 503(5):627–641

Kawai Y (2018) Differential ascending projections from the male rat caudal nucleus of the tractus solitarius: an interface between local microcircuits and global macrocircuits. Front Neuroanat 12:63

Kawai Y, Senba E (1996) Organization of excitatory and inhibitory local networks in the caudal nucleus of tractus solitarius of rats revealed in in vitro slice preparation. J Comp Neurol 373(3):309–321

Koneru B, Bathina CS, Cherry BH, Mifflin SW (2014) Mineralocorticoid receptor in the NTS stimulates saline intake during fourth ventricular infusions of aldosterone. Am J Physiol Regul Integr Comp Physiol 306(1):R61–R66

Krashes MJ, Koda S, Ye C, Rogan SC, Adams AC, Cusher DS, Maratos-Flier E, Roth BL, Lowell BB (2011) Rapid, reversible activation of AgRP neurons drives feeding behavior in mice. J Clin Invest 121(4):1424–1428

Krashes MJ, Shah BP, Madara JC, Olson DP, Strochlic DE, Garfield AS, Vong L, Pei H, Watabe-Uchida M, Uchida N, Liberles SD, Lowell BB (2014) An excitatory paraventricular nucleus to AgRP neuron circuit that drives hunger. Nature 507(7491):238–242

Lesman-Leegte I, Jaarsma T, Sanderman R, Linssen G, van Veldhuisen DJ (2006) Depressive symptoms are prominent among elderly hospitalised heart failure patients. Eur J Heart Fail 8(6):634–640

Loewy A, Spyer K (1990) Central regulation of autonomic functions. Oxford University Press, New York

Luquet S, Perez FA, Hnasko TS, Palmiter RD (2005) NPY/AgRP neurons are essential for feeding in adult mice but can be ablated in neonates. Science 310(5748):683–685

Madisen L, Zwingman TA, Sunkin SM, Oh SW, Zariwala HA, Gu H, Ng LL, Palmiter RD, Hawrylycz MJ, Jones AR, Lein ES, Zeng H (2010) A robust and high-throughput Cre reporting and characterization system for the whole mouse brain. Nat Neurosci 13(1):133–140

Malinow KC, Lion JR (1979) Hyperaldosteronism (Conn's disease) presenting as depression. J Clin Psychiatry 40(8):358–359

Matsuda T, Hiyama TY, Niimura F, Matsusaka T, Fukamizu A, Kobayashi K, Kobayashi K, Noda M (2017) Distinct neural mechanisms for the control of thirst and salt appetite in the subfornical organ. Nat Neurosci 20(2):230–241

McCance RA (1936) Experimental human salt deficiency. Lancet 1:823–830

McKinley MJ, Badoer E, Oldfield BJ (1992) Intravenous angiotensin II induces Fos-immunoreactivity in circumventricular organs of the lamina terminalis. Brain Res 594(2):295–300

Morris MJ, Na ES, Grippo AJ, Johnson AK (2006) The effects of deoxycorticosterone-induced sodium appetite on hedonic behaviors in the rat. Behav Neurosci 120(3):571–579

Murck H, Buttner M, Kircher T, Konrad C (2014) Genetic, molecular and clinical determinants for the involvement of aldosterone and its receptors in major depression. Nephron Physiol 128(1–2):17–25

Naray-Fejes-Toth A, Fejes-Toth G (2007) Novel mouse strain with Cre recombinase in 11beta-hydroxysteroid dehydrogenase-2-expressing cells. Am J Physiol Renal Physiol 292(1):F486–F494

Naray-Fejes-Toth A, Colombowala IK, Fejes-Toth G (1998) The role of 11beta-hydroxysteroid dehydrogenase in steroid hormone specificity. J Steroid Biochem Mol Biol 65(1–6):311–316

Nijenhuis WA, Oosterom J, Adan RA (2001) AgRP(83–132) acts as an inverse agonist on the human-melanocortin-4 receptor. Mol Endocrinol 15(1):164–171

Ollmann MM, Wilson BD, Yang YK, Kerns JA, Chen Y, Gantz I, Barsh GS (1997) Antagonism of central melanocortin receptors in vitro and in vivo by agouti-related protein. Science 278(5335):135–138

Palmiter RD (2018) The parabrachial nucleus: CGRP neurons function as a general alarm. Trends Neurosci 41(5):280–293

Pardridge WM, Mietus LJ (1979) Transport of steroid hormones through the rat blood-brain barrier. Primary role of albumin-bound hormone. J Clin Invest 64(1):145–154

Parvizi J, Damasio A (2001) Consciousness and the brainstem. Cognition 79(1–2):135–160

Price JL, Drevets WC (2012) Neural circuits underlying the pathophysiology of mood disorders. Trends Cogn Sci 16(1):61–71

Reincke M (2018) Anxiety, depression, and impaired quality of life in primary aldosteronism: why we shouldn't ignore it! J Clin Endocrinol Metab 103(1):1–4

Resch JM, Fenselau H, Madara JC, Wu C, Campbell JN, Lyubetskaya A, Dawes BA, Tsai LT, Li MM, Livneh Y, Ke Q, Kang PM, Fejes-Toth G, Naray-Fejes-Toth A, Geerling JC, Lowell BB (2017) Aldosterone-sensing neurons in the NTS exhibit state-dependent pacemaker activity and drive sodium appetite via synergy with angiotensin II signaling. Neuron 96(1):190–206 **(e197)**

Robson AC, Leckie CM, Seckl JR, Holmes MC (1998) 11 Beta-hydroxysteroid dehydrogenase type 2 in the postnatal and adult rat brain. Brain Res Mol Brain Res 61(1–2):1–10

Roland BL, Li KX, Funder JW (1995) Hybridization histochemical localization of 11 beta-hydroxysteroid dehydrogenase type 2 in rat brain. Endocrinology 136(10):4697–4700

Rowland NE, Fregly MJ (1988) Characteristics of thirst and sodium appetite in mice (Mus musculus). Behav Neurosci 102(6):969–974

Rutledge T, Reis VA, Linke SE, Greenberg BH, Mills PJ (2006) Depression in heart failure a meta-analytic review of prevalence, intervention effects, and associations with clinical outcomes. J Am Coll Cardiol 48(8):1527–1537

Sakai RR, Ma LY, Zhang DM, McEwen BS, Fluharty SJ (1996) Intracerebral administration of mineralocorticoid receptor antisense oligonucleotides attenuate adrenal steroid-induced salt appetite in rats. Neuroendocrinology 64(6):425–429

Sakai RR, McEwen BS, Fluharty SJ, Ma LY (2000) The amygdala: site of genomic and nongenomic arousal of aldosterone-induced sodium intake. Kidney Int 57(4):1337–1345

Saper CB (2016) The house alarm. Cell Metab 23(5):754–755

Sawchenko PE, Brown ER, Chan RK, Ericsson A, Li HY, Roland BL, Kovacs KJ (1996) The paraventricular nucleus of the hypothalamus and the functional neuroanatomy of visceromotor responses to stress. Prog Brain Res 107:201–222

Sequeira SM, Geerling JC, Loewy AD (2006) Local inputs to aldosterone-sensitive neurons of the nucleus tractus solitarius. Neuroscience 141(4):1995–2005

Shields AD, Wang Q, Winder DG (2009) alpha2A-adrenergic receptors heterosynaptically regulate glutamatergic transmission in the bed nucleus of the stria terminalis. Neuroscience 163(1):339–351

Shin JW, Geerling JC, Loewy AD (2008) Inputs to the ventrolateral bed nucleus of the stria terminalis. J Comp Neurol 511(5):628–657

Shin JW, Geerling JC, Loewy AD (2009) Vagal innervation of the aldosterone-sensitive HSD2 neurons in the NTS. Brain Res 1249:135–147

Shin JW, Geerling JC, Stein MK, Miller RL, Loewy AD (2011) FoxP2 brainstem neurons project to sodium appetite regulatory sites. J Chem Neuroanat 42(1):1–23

Simpson JB, Routtenberg A (1978) Subfornical organ: a dipsogenic site of action of angiotensin II. Science 201(4353):379–381

Song K, Allen AM, Paxinos G, Mendelsohn FA (1992) Mapping of angiotensin II receptor subtype heterogeneity in rat brain. J Comp Neurol 316(4):467–484

Sonino N, Fallo F, Fava GA (2006) Psychological aspects of primary aldosteronism. Psychother Psychosom 75(5):327–330

Sonino N, Tomba E, Genesia ML, Bertello C, Mulatero P, Veglio F, Fava GA, Fallo F (2011) Psychological assessment of primary aldosteronism: a controlled study. J Clin Endocrinol Metab 96(6):E878–E883

Stornetta RL, Hawelu-Johnson CL, Guyenet PG, Lynch KR (1988) Astrocytes synthesize angiotensinogen in brain. Science 242(4884):1444–1446

Sunn N, McKinley MJ, Oldfield BJ (2003) Circulating angiotensin II activates neurones in circumventricular organs of the lamina terminalis that project to the bed nucleus of the stria terminalis. J Neuroendocrinol 15(8):725–731

Szabo NE, da Silva RV, Sotocinal SG, Zeilhofer HU, Mogil JS, Kania A (2015) Hoxb8 intersection defines a role for Lmx1b in excitatory dorsal horn neuron development, spinofugal connectivity, and nociception. J Neurosci 35(13):5233–5246

Terenzi MG, Ingram CD (1995) A combined immunocytochemical and retrograde tracing study of noradrenergic connections between the caudal medulla and bed nuclei of the stria terminalis. Brain Res 672(1–2):289–297

Tindell AJ, Smith KS, Pecina S, Berridge KC, Aldridge JW (2006) Ventral pallidum firing codes hedonic reward: when a bad taste turns good. J Neurophysiol 96(5):2399–2409

Tong Q, Ye CP, Jones JE, Elmquist JK, Lowell BB (2008) Synaptic release of GABA by AgRP neurons is required for normal regulation of energy balance. Nat Neurosci 11(9):998–1000

Ueda K, Okamura N, Hirai M, Tanigawara Y, Saeki T, Kioka N, Komano T, Hori R (1992) Human P-glycoprotein transports cortisol, aldosterone, and dexamethasone, but not progesterone. J Biol Chem 267(34):24248–24252

Uhr M, Holsboer F, Muller MB (2002) Penetration of endogenous steroid hormones corticosterone, cortisol, aldosterone and progesterone into the brain is enhanced in mice deficient for both mdr1a and mdr1b P-glycoproteins. J Neuroendocrinol 14(9):753–759

Velema MS, de Nooijer AH, Burgers VWG, Hermus A, Timmers H, Lenders JWM, Husson O, Deinum J (2017) Health-related quality of life and mental health in primary aldosteronism: a systematic review. Horm Metab Res 49(12):943–950

Verstegen AMJ, Vanderhorst V, Gray PA, Zeidel ML, Geerling JC (2017) Barrington's nucleus: neuroanatomic landscape of the mouse "pontine micturition center". J Comp Neurol

Walker DL, Toufexis DJ, Davis M (2003) Role of the bed nucleus of the stria terminalis versus the amygdala in fear, stress, and anxiety. Eur J Pharmacol 463(1–3):199–216

Wu Q, Boyle MP, Palmiter RD (2009) Loss of GABAergic signaling by AgRP neurons to the parabrachial nucleus leads to starvation. Cell 137(7):1225–1234

Zardetto-Smith AM, Beltz TG, Johnson AK (1994) Role of the central nucleus of the amygdala and bed nucleus of the stria terminalis in experimentally-induced salt appetite. Brain Res 645(1–2):123–134

Zeisel A, Hochgerner H, Lonnerberg P, Johnsson A, Memic F, van der Zwan J, Haring M, Braun E, Borm LE, La Manno G, Codeluppi S, Furlan A, Lee K, Skene N, Harris KD, Hjerling-Leffler J, Arenas E, Ernfors P, Marklund U, Linnarsson S (2018) Molecular architecture of the mouse nervous system. Cell 174(4):999–1014 **(e1022)**

Zhang ZH, Kang YM, Yu Y, Wei SG, Schmidt TJ, Johnson AK, Felder RB (2006) 11beta-hydroxysteroid dehydrogenase type 2 activity in hypothalamic paraventricular nucleus modulates sympathetic excitation. Hypertension 48(1):127–133